DOI: 10.1093/jnci/djr156
Advance Access publication on June 8, 2011.

ARTICLE

Identification of an Inhibitor of the EWS-FLI1 Oncogenic Transcription Factor by High-Throughput Screening

Patrick J. Grohar, Girma M. Woldemichael, Laurie B. Griffin, Arnulfo Mendoza, Qing-Rong Chen, Choh Yeung, Duane G. Currier, Sean Davis, Chand Khanna, Javed Khan, James B. McMahon, Lee J. Helman

Manuscript received August 11, 2010; revised March 14, 2011; accepted April 11, 2011.

Correspondence to: Patrick J. Grohar, MD, PhD, Pediatric Oncology Branch, National Cancer Institute, National Institutes of Health, 10 Center Dr-MSC 1104, 10 CRC 1W-3816, Bethesda, MD 20892-1104 (e-mail: groharp@mail.nih.gov).

Background Chromosomal translocations generating oncogenic transcription factors are the hallmark of a variety of tumors, including many sarcomas. Ewing sarcoma family of tumors (ESFTs) are characterized by the t(11;22)(q24;q12) translocation that generates the Ewing sarcoma breakpoint region 1 and Friend leukemia virus integration 1 (EWS-FLI1) fusion transcription factor responsible for the highly malignant phenotype of this tumor. Although continued expression of EWS-FLI1 is believed to be critical for ESFT cell survival, a clinically effective small-molecule inhibitor remains elusive likely because EWS-FLI1 is a transcription factor and therefore widely felt to be "undruggable."

Methods We developed a high-throughput screen to evaluate more than 50 000 compounds for inhibition of EWS-FLI1 activity in TC32 ESFT cells. We used a TC32 cell–based luciferase reporter screen using the EWS-FLI1 downstream target NR0B1 promoter and a gene signature secondary screen to sort and prioritize the compounds. We characterized the lead compound, mithramycin, based on its ability to inhibit EWS-FLI1 activity in vitro using microarray expression profiling, quantitative reverse transcription–polymerase chain reaction, and immunoblot analysis, and in vivo using immunohistochemistry. We studied the impact of this inhibition on cell viability in vitro and on tumor growth in ESFT xenograft models in vivo (n = 15–20 mice per group). All statistical tests were two-sided.

Results Mithramycin inhibited expression of EWS-FLI1 downstream targets at the mRNA and protein levels and decreased the growth of ESFT cells at half maximal inhibitory concentrations between 10 (95% confidence interval [CI] = 8 to 13 nM) and 15 nM (95% CI = 13 to 19 nM). Mithramycin suppressed the growth of two different ESFT xenograft tumors and prolonged the survival of ESFT xenograft–bearing mice by causing a decrease in mean tumor volume. For example, in the TC32 xenograft model, on day 15 of treatment, the mean tumor volume for the mithramycin-treated mice was approximately 3% of the tumor volume observed in the control mice (mithramycin vs control: 69 vs 2388 mm^3, difference = 2319 mm^3, 95% CI = 1766 to 2872 mm^3, $P < .001$).

Conclusion Mithramycin inhibits EWS-FLI1 activity and demonstrates ESFT antitumor activity both in vitro and in vivo.

J Natl Cancer Inst 2011;103:962–978

Oncogenic transcription factors generated by chromosomal translocations are found in all types of cancer ranging from leukemias to solid tumors of both epithelial and mesenchymal origin. In most cases, these transcription factors are integral to malignant transformation and maintenance of the oncogenic phenotype suggesting that these proteins would be ideal drug targets (1–3). However, it has been challenging to identify small-molecule inhibitors of these transcription factors and, in general, these proteins have been described as "undruggable" targets.

The Ewing sarcoma family of tumors (ESFT) comprises a group of highly malignant bone tumors of childhood. Approximately 85% of these tumors are characterized by the t(11;22)(q24;q12) translocation, which generates the highly dysregulated EWS-FLI1 transcription factor that is believed to be responsible for malignant transformation and progression (4–15). Multiple studies have shown that knockdown of EWS-FLI1 with either small interfering RNA (siRNA) or antisense DNA decreases viability as well as tumorigenicity in orthotopic mouse models (9,10,16–18). This finding has led to a variety of efforts to identify a small-molecule inhibitor of the EWS-FLI1 transcription factor (19,20).

Here, we describe the development and implementation of a high-throughput screening strategy to identify inhibitors of the EWS-FLI1 transcription factor. We used a high-throughput screen that used a promoter-based primary screen for luciferase expression and a multiplex polymerase chain reaction (PCR) secondary screen of EWS-FLI1–induced downstream targets to evaluate more than 50 000 compounds including many natural products. The top candidate from this screen was mithramycin, a

drug that binds GC-rich regions of the genome and regulates the expression of specific genes including *SRC*, *MYC*, and *MDR1* often by inhibiting the SP1 family of transcription factors (21–26). In this report, we studied the effects of mithramycin on expression of EWS-FLI1 downstream targets in ESFT cells and on tumor growth in vivo.

Materials and Methods

Cell Lines, Cell Culture, and Reagents

All cell lines are patient derived. The cells were maintained in growth medium (RPMI 1640 [Invitrogen, Carlsbad, CA] with 10% fetal bovine serum [Sigma-Aldrich, St Louis, MO], 100 U/mL penicillin and 100 μg/mL streptomycin [Invitrogen], and 2 mM L-glutamine [Invitrogen]). The cells were maintained at 80% or less confluency at 37°C in an atmosphere of 5% CO. The osteosarcoma cell lines MNNG-HOS and U20S have been described previously (27,28). Breast carcinoma MD-MBA-231 and MCF7 cells were the kind gift of Dr Patricia Steeg (National Cancer Institute, Bethesda, MD) and have been previously characterized (29,30). Ovarian cancer SKOV-3 cells were obtained from American Type Culture Collection (Manassas, VA). ESFT cell lines TC32, TC71, A673, CHLA9, and TC167 were the gift of Tim Triche (The Saban Research Hospital, Children's Hospital of Los Angeles, Los Angeles, CA) and were confirmed by short-tandem repeat genotyping (http://strdb.cogcell.com/). EW8 ESFT cells were the gift of Peter Houghton (Nationwide Children's Hospital, Columbus, OH) and have been characterized previously (31). The identities of all ESFT cell lines were confirmed by reverse transcription–PCR (RT-PCR) using primers specific for the translocation. We did not independently confirm the identities of the other cell lines. The expression of EWS-FLI1 was confirmed routinely by RT-PCR for all ESFT cell lines.

Chemical Library

To screen for inhibitors of the EWS-FLI1 transcription factor, we used a chemical library containing more than 50 000 compounds that were isolated from natural product extracts, purchased, or acquired through collaborations by the Molecular Targets Laboratory at the National Cancer Institute at Frederick (Frederick, MD). Information about the source of the library and the individual compounds is available online at http://dtp.nci.nih.gov/branches/npb/repository.html. To develop and validate the high-throughput screen, we used a test set comprising 6500 compounds that were selected to reflect the diversity of the 50 000-compound library to assess the consistency and reproducibility of the high-throughput assay.

Luciferase Reporter Constructs

The NR0B1 promoter was amplified by PCR from genomic DNA isolated from TC32 cells with primers containing recognition sites for *Kpn*I and *Nhe*I restriction enzymes (Supplementary Table 1, available online) and ligated into a TOPO-TA shuttle vector (Invitrogen). The resulting plasmid was amplified in DH5α *Escherichia coli*, purified, and digested with *Kpn*I and *Nhe*I (New England Biolabs, Ipswich, MA) in buffer I containing bovine serum albumin as per the manufacturer's protocol. The NR0B1 promoter–containing fragment was purified and cloned into pGL4.18 (Promega, Madison, WI), a reporter plasmid containing the firefly luciferase gene. The resulting plasmid (NR0B1-Luc) was linearized with *Sal*I (New England Biolabs) and introduced into TC32 cells in the presence of buffer R with the use of program O-17 and an Amaxa Nucleofector System (Lonza, Basel, Switzerland) according to the manufacturer's instructions.

The cytomegalovirus (CMV) promoter was PCR amplified from pGL4.75 (Promega) with primers containing the appropriate In-Fusion cloning 2.0 (Clontech, Mountain View, CA) recombination sites, which were designed using the manufacturer's online software (Supplementary Table 1, available online). The PCR product was purified and cloned into the *Nhe*I site of pGL4.18. The resulting plasmid (CMV-Luc) was introduced into TC32 cells by nucleofection using buffer R, program O-17, and the Amaxa System (Lonza).

High-Throughput Screen Assay Development

We generated separate stable TC32 cell lines expressing the NR0B1 reporter (NR0B1-Luc) or the CMV reporter (CMV-Luc)

CONTEXT AND CAVEATS

Prior knowledge

The Ewing sarcoma family of tumors (ESFTs) is characterized by a chromosomal translocation that generates EWS-FLI1, an oncogenic fusion transcription factor whose continued expression is believed to be critical for ESFT cell survival.

Study design

A high-throughput promoter-based screen was conducted to identify compounds that inhibit EWS-FLI1 activity in ESFT TC32 cells. A TC32 cell–based luciferase reporter screen using the EWS-FLI1 downstream target NR0B1 promoter and a gene signature secondary screen was used to sort and prioritize the compounds. The lead compound identified in the screen—mithramycin—was characterized by microarray expression profiling, quantitative reverse transcriptase–polymerase chain reaction, immunoblot analysis, immunohistochemistry, and in ESFT xenograft models.

Contribution

Mithramycin blocked expression of EWS-FLI1 downstream targets in vitro at both the RNA and protein levels and suppressed protein expression of a well-characterized downstream target, NR0B1, in vivo. Mithramycin inhibited ESFT cell growth in vitro with IC_{50} values ranging from 10 to 15 nM and suppressed the growth of ESFT xenografts in vivo.

Implications

Mithramycin inhibits EWS-FLI1 activity and demonstrates ESFT antitumor activity both in vitro and in vivo.

Limitations

The screen and subsequent experiments were all conducted in cell lines and xenografts of those cell lines. There was no independent verification of the authenticity of the non-ESFT cell lines used in this study. The investigators were not blinded to the treatment groups in the mouse experiments. Only one assay for apoptosis was performed.

From the Editors

by expanding single-cell TC32 clones under selective pressure in medium containing G418 (Sigma-Aldrich) at a concentration of 0.5 mg/mL. To ensure that these clones were suitable for high-throughput screening, we selected cells that produced a strong luciferase signal with minimal well-to-well variability. The cells were optimized for cell seeding density, automation in cell plating and liquid handling, length of incubation before treatment, reporter half-life, and length of incubation after treatment for the high-throughput screening assay. The assay was validated for consistency and reproducibility by performing three separate screens of the 6500-compound test set (see above), which yielded a high correlation coefficient (median $R^2 = 0.9$; range = 0.87−0.91).

High-Throughput Screen

The 50 000-compound library was subjected to a high-throughput screen to detect compounds that decreased expression of the NR0B1-Luc reporter but had no effect on expression of the CMV-Luc reporter or on cell viability in three separate screens that were run in parallel. Test compounds were stored at various concentrations in 100% dimethyl sulfoxide (DMSO) at −20°C in 384-well plates, thawed just before use, and prepared in stock dilution plates at a concentration of 100 μM in growth medium in a 384-well dilution plate using a Biomek-FX liquid handler (Beckman Coulter, Brea, CA). TC32 NROB1-Luc cells and TC32 CMV-Luc cells were dispensed into opaque-bottom white 384-well assay plates (PerkinElmer, Waltham, MA) at 5000 cells per well in 27 μL growth medium using a μFill dispenser (BioTek, Winooski, VT) for the luciferase reporter assay. TC32 NROB1-Luc cells were similarly dispensed into clear 384-well assay plates (PerkinElmer) for the cell viability assay. The cells were incubated for 4 hours at 37°C, and then 3 μL of each test compound from the 100-μM stock dilution plate was transferred into assay plates (final concentration of test compounds was 10 μM and final concentration of DMSO was ≤1%). The cells were incubated for 24 hours at 37 °C. We added 30 μL of SteadyLite luciferase assay reagent (PerkinElmer) to each well of an opaque-bottom white assay plate and measured luciferase reporter activity with the use of a BMG Labtech plate reader (Offenburg, Germany) in the luminescence mode. Cell viability was assessed in parallel by adding XTT reagent to the clear assay plate (10 μL per well; Developmental Therapeutics Program, National Cancer Institute, Frederick, MD) and measuring absorbance at 450 nm of the colored formazan product of XTT metabolism with the use of a PerkinElmer Wallac plate reader in the absorbance mode. All assay plates contained 16 wells each of the positive control compound [actinomycin D; chosen as a general transcription inhibitor based on performance in previous assays (32)] and the negative control compound (DMSO). Routine measurement of assay performance using these controls via the calculation of the Z-factor (33) for each screening plate revealed a Z' of 0.78–0.9, indicating that the screening assay performed well during high-throughput screening. The following criteria were used to define hits in the primary screen: 1) decrease luciferase expression in TC32 NR0B1-Luc cells to less than 46% of solvent control, 2) maintain greater than 80% of control reporter activity in TC32 CMV-Luc cells, and 3) decrease cell viability, as measured by an XTT assay, by less than 20%. Cut points were chosen to yield a manageable number of compounds for secondary screening with the premise of expanding the number if an EWS-FLI1 inhibitor was not identified. A total of 150 compounds fulfilled all three criteria and, along with the 50 most cytotoxic compounds as determined by the XTT cell viability assay, were considered for secondary screening.

Compound Sort and Prioritization for the Secondary Screen

The 200 compounds identified in the high-throughput screen were subsequently evaluated for luciferase expression and cell viability in the same manner as for the primary screen (described in detail above) over six 10-fold dilutions ranging from 10 μM to 0.1 nM to prioritize them for further screening. The compounds were sorted in descending order according to a score, X, which was the sum of the $\log_2$ difference between the normalized luciferase expression for the CMV-driven luciferase and the NR0B1-normalized luciferase expression over all six concentrations:

$$\text{Score } X = \Sigma[((\log_2(\text{CMV-Luc}) - \log_2(\text{NR0B} - 1\ \text{Luc}))10\ \text{nM} + \ldots\ldots\ldots (\log(\text{CMV-Luc}) - \log(\text{NR0B} - 1\ \text{Luc}))0.1\ \text{nM}]$$

We selected the 43 compounds with the highest scores for secondary screening based on their ability to decrease luciferase expression in TC32 NR0B1-Luc cells, while maintaining luciferase expression in TC32 CMV-Luc cells when diluted 10-fold to a final concentration of 1 μM.

Identification of EWS-FLI1 Downstream Targets

To compile a list of EWS-FLI1 downstream targets to develop the secondary screen, we identified the following: 1) genes that were highly expressed in tumor samples from ESFT patients, 2) genes whose expression was induced with forced EWS-FLI1 expression in mesenchymal progenitor cells [the presumed cell of origin of Ewing sarcoma (7,34–37)], and 3) genes whose expression decreased with siRNA knockdown of EWS-FLI1.

Highly expressed genes in ESFT tumor tissue were identified from two pediatric cancer patient sample datasets (available at http://home.ccr.cancer.gov/oncology/oncogenomics). We first selected genes whose expression was twofold higher in ESFT tissue samples compared with other tumor types and normal tissue samples ($P < .001$; Student t test). We then retained only the genes whose expression was induced twofold by EWS-FLI1 expression in mesenchymal progenitor cells relative to a green fluorescent protein (GFP) control ($P < .01$; Student t test). Finally, we eliminated genes whose expression in ESFT cell lines did not decrease with siRNA knockdown of EWS-FLI1 (38), yielding a list of 28 genes induced by EWS-FLI1 (Figure 1, B). We used a subset of these genes in the final multiplex PCR assay of EWS-FLI1 downstream targets as described below.

Lentivirus Transduction of Human Mesenchymal Progenitor Cells

Mesenchymal progenitor cells were isolated from bone marrow samples from adult orthopedic patients in the laboratory of Dr Rocky Tuan in the Cartilage Biology and Orthopedics branch of the National Institute of Arthritis and Musculoskeletal and Skin Diseases (Bethesda, MD) and transduced with a lentivirus containing EWS-FLI1 (generated by Betty Conde in the core facility at National Cancer Institute-Frederick, Frederick, MD) at a

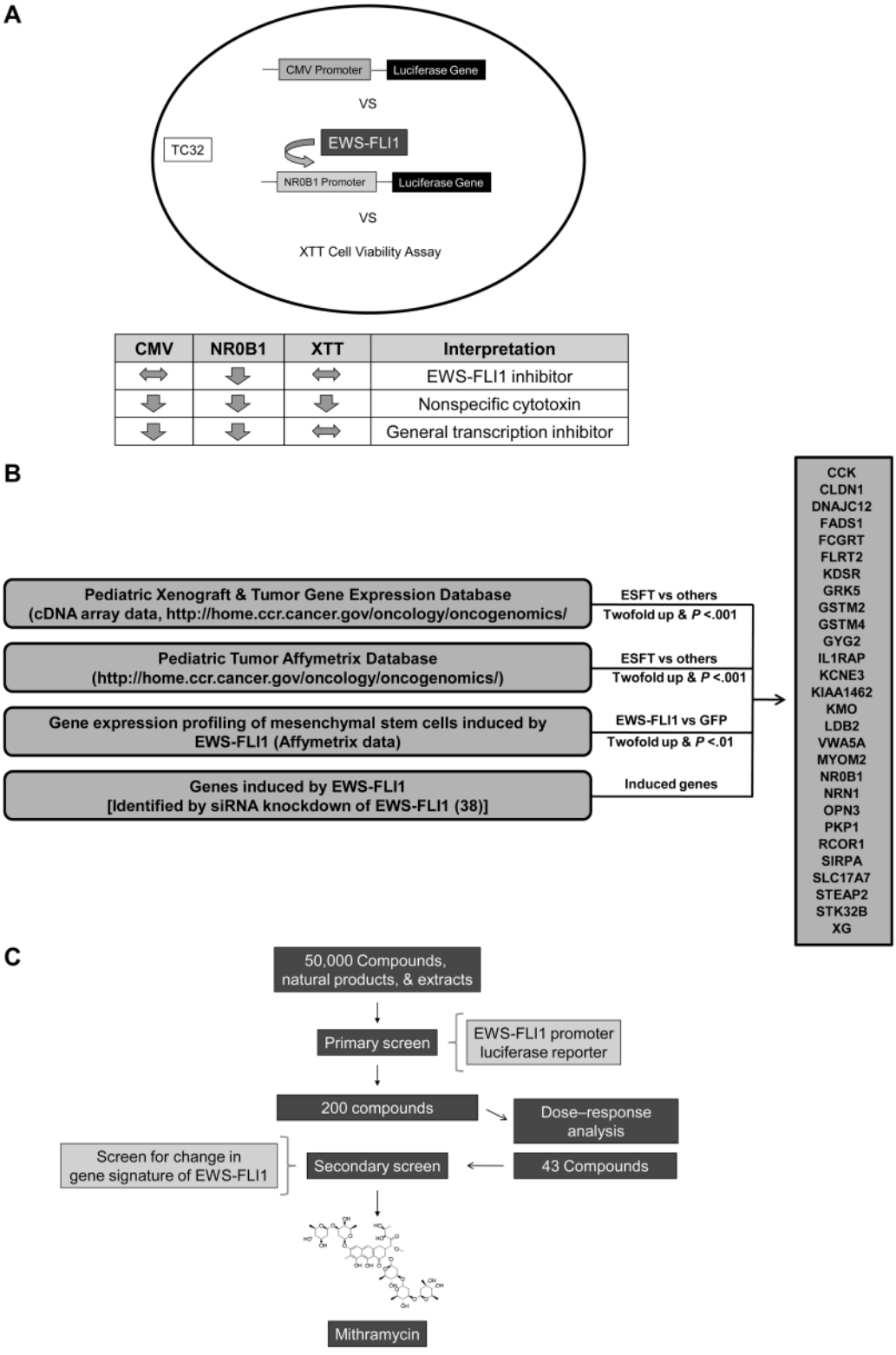

Figure 1. High-throughput luciferase-based primary screen and multiplex polymerase chain reaction secondary screen of a library of more than 50 000 compounds. **A**) Primary screen design. A cell-based luciferase primary screen included the EWS-FLI1 downstream target NR0B1 promoter and a CMV promoter, which was used to control for nonspecific cytotoxins and general transcription inhibitors. **Downward arrows** indicate decreased activity of the luciferase reporter construct and the **left–right arrows** represent no change in activity. **B**) List of EWS-FLI1 downstream targets used for the secondary screen. Novel list of EWS-FLI1–induced target genes comprising genes that are highly expressed in Ewing sarcoma patient tissue, that suppress with EWS-FLI1 siRNA knockdown, and that are induced when EWS-FLI1 is expressed in the presumed cell of origin. This list was used to generate the gene list used in the multiplex polymerase chain reaction assay. See Supplementary Table 1 (available online) for full gene names. **C**) Summary of screen design. The summary of the screen highlights the method used to identify mithramycin starting from more than 50 000 pure compounds to the lead compound. CMV = cytomegalovirus; ESFT = Ewing sarcoma family of tumors; siRNA = small interfering RNA.

multiplicity of infection (MOI) of 10 in the presence of 6 μg/mL polybrene to facilitate transduction. RNA was collected from the transduced cells and subjected to microarray expression profiling as described below.

Development of Multiplex PCR Assay of EWS-FLI1 Downstream Targets

EWS-FLI1 alters the expression of more than 500 genes (7). However, our primary screen only evaluated the expression of one downstream target via promoter-driven luciferase expression. Therefore, to ensure that compounds identified in the primary screen block EWS-FLI1 activity, we developed a multiplex PCR assay that allowed simultaneous measurement of the expression of multiple downstream targets of EWS-FLI1. Although we had developed a list of 28 downstream targets of EWS-FLI1 as described above, it was not possible to include all 28 genes in the multiplex PCR assay. The assay uses capillary electrophoresis to separate gene-specific PCR products. Therefore, each gene has to yield a single clean PCR product that differs in length by at least seven nucleotides from the PCR product of every other gene in the assay and is between 130 and 300 nucleotides in total length. These requirements limit the number of gene targets used in one multiplex assay to, at most, 24 targets. Because we also wanted to include four housekeeping genes—*GAPDH*, *ACTB*, *EEF1A1*, and *PPIA*— as negative controls, a maximum of 20 target genes could be included. We also wanted to include *ID2* and *CAV1*, which are strongly supported as EWS-FLI1 targets in the literature (39,40), even though these genes did not appear in all four datasets used to identify the 28 target genes. This further limited the number of target genes that could be included to 18. We reevaluated each of the genes in our original 28-gene list relative to the other genes on the list and eliminated those with lower expression in primary tumors (ie, *FADS1*, *KCNE3*, *KIAA1462*, *VWA5A*, *NRN1*, and *STK32B*), those with less-pronounced induction in the mesenchymal progenitor cells (ie, *GRK5* and *GYG2*), and those with less-pronounced induction with siRNA knockdown of EWS-FLI1 (ie, *FLRT2*, *KIAA1462*, *VWA5A*, and *OPN3*). The remaining 17 genes were used for assay development. The nine genes that produced the cleanest PCR product of the appropriate size were included in the final assay, along with probes designed to detect expression of EWS-FLI1, CAV1, ID2, and the four housekeeping genes The final assay included 11 EWS-FLI1 target genes (*ID2*, *FCGRT*, *NR0B1*, *STEAP2*, *CAV1*, *LDB2*, *RCOR1*, *KDSR*, *IL1RAP*, *CCK*, and *XG*), a primer pair to amplify Kan^r RNA (which was used as an internal PCR control), a primer pair for EWS-FLI1, and the four housekeeping genes (*PPIA*, *GAPDH*, *ACTB*, and *EEF1A1*). The sequences of the gene-specific primer pairs are listed in Supplementary Table 2 (available online).

Secondary Screen

The 43 compounds identified in the primary screen were evaluated for their ability to suppress expression of EWS-FLI1 downstream targets in the multiplex PCR assay without changing expression of the housekeeping genes. The individual compounds were stored frozen in 10% DMSO at a concentration of 100 μM. The compounds were thawed immediately before use and diluted to a final concentration of 100 nM in growth medium. TC32 NR0B1-Luc cells (140 000 cells per well) were added to a 12-well plate and incubated overnight. The medium was aspirated and replaced with one of the 43 compounds at 100 nM. The cells were incubated for 6 hours, at which point the medium was aspirated, and the cells were washed and lysed in the plate with the addition of RLT buffer (Qiagen, Germantown, MD). RNA was purified using the RNeasy mini kit (Qiagen) and the automated QIAcube RNA purification system (Qiagen) according to the manufacturer's instructions. The RNA was quantitated with the use of a NanoDrop 2000 spectrophotometer (Thermo, Waltham, MA), and only RNA with a ratio of the absorbance at 260 nm to that at 280 nm greater than 2 was used in the assay. RNA was reverse transcribed using gene-specific reverse primers (Supplementary Table 2, available online) and a GeXP Start kit (Beckman Coulter) containing reverse transcriptase, reverse transcriptase buffer, Kan^r reverse transcriptase primer, and Kan^r RNA, which was added to all reactions as an internal PCR control. The reverse transcription reaction was run in triplicate on a Veriti thermocycler (Applied Biosystems, Norwalk, CT) with the following program: 48°C for 1 minute, 37°C for 5 minutes, 42°C for 60 minutes, and 95°C for 5 minutes. The reaction mixture (9.3 μL) was transferred to a second tube for PCR amplification of the cDNA using Thermostart Taq DNA polymerase (Thermo), gene-specific forward primers (Supplementary Table 2, available online), and the GeXP PCR kit, which contained $MgCl_2$ (final concentration 5 mM), deoxynucleoside triphosphates, buffer, and fluorescently labeled nested PCR primers. The PCR program was run on a Veriti thermocycler (Applied Biosystems) with a standard "hot start" program of 95°C for 10 minutes, 94°C for 30 seconds, 55°C for 30 seconds, and 70°C for 1 minute (35 cycles).

The PCR products were separated by capillary electrophoresis with the use of a GenomeLab GeXP device (Beckman Coulter), and the individual PCR products were quantitated based on their peak height as measured by the fluorescent detector in the GeXP instrument. Expression was quantitated by normalizing the peak height of each gene to the Kan^r internal PCR control and to the geometric mean of the four housekeeping genes. This value was subsequently fit to a standard curve using a third-order polynomial equation while maintaining a correlation coefficient (R^2) greater than .99 to yield a final expression value. The standard curve was generated by performing RT-PCR on RNA collected from untreated TC32 cells using the same reagents and protocol that were used for cells treated with the compounds over a range of RNA inputs from 500 to 1 ng.

The compounds were sorted based on their ability to suppress the mRNA expression of each of the EWS-FLI1 downstream targets in the assay. To quantitate the difference in expression for treated vs solvent-treated control cells, we summed the difference in expression for each EWS-FLI1 downstream target evaluated in the assay for each compound using log-transformed data, which yielded a score (Y) for each compound:

$$\text{Score } Y = \Sigma\,[((\log_2(\text{Gene 1control}) - \log_2(\text{Gene 1treated}))... + ...(\log_2(\text{Gene 11control}) - \log_2(\text{Gene 11treated}))]$$

The compounds were subsequently sorted in descending order of Y score (data not shown); the highest scoring compound—mithramycin—was selected for further study.

Quantitative RT-PCR

The goal of the secondary screen was to prioritize the compounds for further study. Because mithramycin was the highest priority compound, we first wanted to confirm that it was able to suppress RNA expression of EWS-FLI1 downstream targets by using the more generally accepted method of quantitative RT-PCR. TC32 cells (120 000 cells per well) were plated in triplicate in 12-well plates and allowed to recover overnight. The growth medium was subsequently removed and replaced with growth medium containing 100 nM mithramycin or solvent control (0.01% phosphate-buffered saline [PBS] in growth medium). RNA was collected using an RNeasy kit and a QIAcube (Qiagen) as described above. RNA (500 ng) was reverse transcribed using a high-capacity reverse transcriptase kit (Applied Biosystems), which contains 10× RT buffer, 25 × dNTPs, 10× random RT primers, and reverse transcriptase in a Veriti thermocycler (Applied Biosystems) according to the following program: 25°C for 10 minutes, 37°C for 60 minutes, and 85°C for 5 minutes. The cDNA product (100 ng) was subsequently PCR amplified using the primers developed for the multiplex assay, which are known to produce one clean cDNA product of the target genes (*CCK*, *ID2*, *LDB2*, *NR0B1*, *RCOR1*, and *GAPDH*) by quantitative PCR using a Sybr green kit (Applied Biosystems) and the CFX 96 Real Time System (Bio Rad, Hercules, CA) according to the following program: 95°C for 10 minutes, 95°C for 15 minutes, 55°C for 15 minutes, and 72°C for 1 minute for 40 cycles. Expression was determined by comparing the average threshold cycle (Ct) for the three 100 nM mithramycin-treated replicates to the average Ct for the three solvent control–treated replicates by using the Pfaffl equation (36) to determine fold change in expression for each gene. The average Ct was determined by normalizing the Ct of *CCK*, *ID2*, *LDB2*, *NR0B1*, and *RCOR1* to that of *GAPDH* (41). The entire experiment was repeated two more times with similar results, and the data are presented as the average for the three independent experiments that included eight replicate samples.

Mithramycin

Mithramycin was purchased from Tocris Bioscience (Bristol, UK), dissolved as a 1 mg/mL stock solution in PBS, and frozen in aliquots for use in the in vitro and in vivo experiments. For in vivo experiments, an aliquot of the 1 mg/mL stock solution was diluted to the appropriate concentrations in PBS, and the dilutions were frozen and stored at −80°C to avoid repeated freeze–thaw cycles. For in vitro experiments, an aliquot of the 1 mg/mL stock solution was diluted with medium immediately before use.

Cell Proliferation Assays

The viability of all cell lines in the presence and absence of mithramycin was determined with the use of the CellTiter 96 3-(4, 5-dimethylthiazol-2-yl)-5-(3-carboxymethoxyphenyl)-2-(4-sulfophenyl)-2H-tetrazolium, inner salt (MTS) assay (Promega). Cells were plated in a 96-well plate (5000 cells per well) and incubated overnight. Mithramycin was diluted in a medium over a range of concentrations from 500 to 0.5 nM and added to the cells. The cells were incubated for 48 hours, and 20 μL of CellTiter 96 reagent (Promega) was added to each well and the cells were incubated for 1 hour at 37°C. The color change produced by the bioreduction of the MTS reagent was measured by reading the percent transmittance at 490 nm with the use of a VersaMax 96-well plate reader (Molecular Devices, Sunnyvale, CA) and plotted against a standard curve previously generated for each individual cell line over a range of cell numbers to yield an estimate of the cell number. The cell number was evaluated as a function of drug concentration by nonlinear regression with the use of Prism 4.0 software (GraphPad Software Inc, La Jolla, CA) to determine the concentration of half-maximal inhibition of viability (IC_{50}). Each experiment was performed with three to six replicates and two to five independent experiments per cell line.

Immunoblot Analysis

TC32 and TC71 cells (1.5×10^6) were plated in 10 cm^2 dishes and incubated overnight. The medium was aspirated and the cells were incubated with freshly diluted mithramycin at the times and concentrations specified for each experiment. The cells were scraped into PBS using a cell lifter (Fisher Scientific, Waltham, MA) and centrifuged (233*g*) for 2 minutes. The cells were washed with an additional 1 mL of PBS, centrifuged (2000*g*) for 2 minutes, and lysed in 4% LDS buffer (Sigma-Aldrich) containing Complete Mini Protease Inhibitor Cocktail (one tablet per 10 mL LDS buffer; Roche, Mannheim, Germany). The protein concentration of the lysates was determined by the bicinchoninic acid (BCA) assay (Pierce, Waltham, MA). Cell lysates (25 μg protein per sample) were resolved on a 4%–12% Bis-Tris gel (Invitrogen) in 1× NuPage 3-(N-Morpholino)propanesulfonic acid (MOPS) sodium dodecyl sulfate (SDS) buffer or 2-(N-Morpholino)ethanesulfonic acid (MES) SDS buffer (Invitrogen) and transferred to nitrocellulose membranes using 1× NuPage transfer buffer (Invitrogen) with 20% methanol. The membranes were subsequently probed with the following antibodies: rabbit monoclonal anti-ID2 (1:1000 dilution; Cell Signaling, Danvers, MA), mouse monoclonal anti-FLI1 (1.5 μg/mL; BD biosciences, Franklin Lakes, NJ), rabbit polyclonal anti-NR0B1 (1:1000 dilution; Abcam, Cambridge, UK), rabbit polyclonal anti-β-actin (1:10 000 dilution; Abcam), mouse monoclonal anti-cleaved PARP (1:1000 dilution; Cell Signaling), mouse monoclonal anti-phospho-histone H2A.X (ser 139) (γH2AX) (1:1000 dilution; Upstate, Billerica, MA), mouse monoclonal anti-p53 (1:1000 dilution; Cell Signaling), rabbit monoclonal anti-p21 (1:1000 dilution; Cell Signaling), and rabbit polyclonal anti-phos-P53 (ser 15) (1:1000 dilution; Cell Signaling). The membranes were incubated with horseradish peroxidase (HRP)–conjugated goat polyclonal anti-mouse or anti-rabbit immunoglobulin (IgG) (1:2000 dilution; Pierce), and bound antibody was visualized on film using an ECL Western Blotting Analysis System (Amersham, Buckinghamshire, UK).

Confocal Microscopy

TC32 cells (20 000 cells) were plated in a Lab Tek II chamber slide with cover (Nunc, Rochester, NY) and incubated overnight. The medium was aspirated and the cells were treated with 100 nM mithramycin for 24 hours, fixed in 4% paraformaldehyde in PBS, washed, and permeabilized in 1% Triton X-100. The cells were incubated with 10% goat serum to block nonspecific protein binding and probed with a mouse monoclonal anti-phospho-histone H2A.X (ser 139) antibody (1:200 dilution; Upstate). The cells were incubated with Alexa488-labeled secondary antibody (Millipore, Billerica, MA), mounted in VectaShield mounting medium containing DAPI

(Vector Labs, Burlingame, CA), and viewed with the use of a Zeiss 510 confocal microscope.

Xenograft Experiments

First, we performed an in vivo dose–response experiment to determine the effective dose of mithramycin (ie, the maximum dose of mithramycin that was well tolerated without appreciable toxicity). Five cohorts of SCID-Bg mice (20 mice per group, 4–6 weeks old; Charles River Laboratories, Wilmington, MA) were injected with 2×10^6 TC71 cells per mouse into the left gastrocnemius muscle. Once a tumor with a minimum diameter of 0.5 cm was established, the mice were randomly assigned to receive no treatment or treatment with mithramycin at a dose of 1, 0.5, 0.1, or 0.05 mg/kg body weight on an Monday-Wednesday-Friday (M-W-F) schedule. Two mice in each group were killed by CO_2 asphyxiation on days 2 and 4 after initiation of treatment and their tumor tissue was collected immediately and frozen for later analysis of protein expression by either immunoblotting or immunohistochemistry. The dose–response analysis was performed by plotting the tumor volume for every mouse as a function of dose on day 11 and selecting the most effective dose where minimal toxicity was observed. The lower-dose mithramycin cohorts had fewer mice because some were killed when their tumors reached a diameter of 2 cm.

Once the maximum effective dose without appreciable toxicity was determined to be 1 mg/kg body weight per dose on a M-W-F schedule, three cohorts of female SCID-Bg mice (30 mice per group, 4–6 weeks old; Charles River Laboratories) were injected with either TC32, TC71, or MNNG-HOS cells (2×10^6 cells per mouse) into the left gastrocnemius muscle. Once every mouse that was injected with a particular cell line had established a tumor with a minimum diameter of 0.5 cm, all mice in that group (either bearing TC32, TC71, or MNNG-HOS) were randomly assigned to treatment (n = 15; mithramycin) or control (n = 15; no treatment). Mice in the treated cohorts were subsequently treated by intraperitoneal injection with 1 mg/kg body weight per dose mithramycin or no treatment on a M-W-F schedule and killed by CO_2 asphyxiation when the tumor reached a diameter of 2 cm. Survival analysis includes 12 mice at risk because three mice in each cohort were collected for tumor tissue analysis 12 days after the start of treatment and therefore were excluded from the analysis.

Each tumor was measured three times per week, and tumor volume was determined using the equation $(D \times d^2)/6 \times 3.12$, where D is the maximum diameter and d is the minimum diameter. Tumor volumes for all mice in each xenograft-treatment group (excluding the mice that were killed on the predetermined schedule) were averaged to yield the mean tumor volume for the corresponding group. The experiments were approved by the Animal Care and Use Committee of the National Cancer Institute. Investigators were not blinded to the treatment groups.

Immunohistochemistry of Xenograft Tumor Tissue

The tumor tissue was fixed in 10% formalin, sectioned (10-μm-thick sections), and stained with hematoxylin–eosin (American Histo Labs, Gaithersburg, MD). Additional 10-μm sections were obtained for immunohistochemistry and deparaffinized with xylene, 100% ethanol, and 95% ethanol. Antigen retrieval was performed with citrate buffer (DakoCytomation, Glostrup, Denmark). The sections were incubated with 3% hydrogen peroxide to quench peroxidase activity, followed by incubation with 5% goat serum to block nonspecific protein binding and incubation overnight with rabbit polyclonal anti-NR0B1 (6 μg/mL; Abcam). Sections were subsequently labeled using biotinylated goat anti-rabbit secondary IgG antibody and streptavidin-conjugated horseradish peroxidase (Dako). The sections were stained with hematoxylin, washed, and mounted with mounting medium (Dako). Images were obtained in the National Institutes of Health core imaging facility.

Microarray Analysis of EWS-FLI1 Downstream Targets

TC32 and TC71 cells were plated in triplicate (1.5×10^6 cells per replicate) and incubated overnight. The cells were treated with 100 nM mithramycin for 6 hours, washed, and lysed in 1 mL of TRIzol reagent (Invitrogen). The lysates were subjected to chloroform extraction and centrifuged at 16 000*g* at 4°C. The aqueous layer was collected, mixed with an equal volume of 70% ethanol, and total RNA was purified using the RNeasy protocol (Qiagen) as per the manufacturer's instructions. RNA integrity was determined with the use of a Bioanalyzer (Agilent, Santa Clara, CA) according to the manufacturer's instructions. Gene expression profiling was performed using the GeneChip Human Genome U133 Plus 2.0 microarray (Affymetrix, Santa Clara, CA). RNA was in vitro transcribed, fragmented, hydridized, and stained using the appropriate GeneChip kits (Affymetrix) as per the manufacturer's instructions. The CEL files were exported from Affymetrix GCOS software and normalized with RMA-sketch from Affymetrix Power Tools.

Statistical Methods

Data are presented as mean values with 95% confidence intervals (CIs). The Student *t* test was performed to determine the statistical significance of differences between the treated and the control groups for the PCR results and the tumor volumes in the mouse studies. The survival analysis for the mouse experiment was performed using Kaplan–Meier analysis, log-rank test, and the Prism 4.0 software package (GraphPad Software Inc). A *P* value less than .05 was considered statistically significant. All statistical tests were two-sided. Expression profiling was analyzed using GCOS software and normalized with RMA-sketch from Affymetrix Power Tools (42). The gene set enrichment analysis (GSEA) method (http://www.broad.mit.edu/gsea/) was applied to investigate the enrichment of the list of EWS-FLI1–induced downstream targets. GSEA analysis was completed with a weighted enrichment statistic and genes were ranked using the $\log_2$ ratio of expression for mithramycin-treated cells to control cells. The limma bioconductor package was used to construct a two-factor linear model between control and treatment groups. Enrichment of the EWS-FLI1 gene list was tested using the geneSetTest function from the limma package (43).

Results

The Primary and Secondary Screens

The goal of this study was to identify inhibitors of the EWS-FLI1 transcription factor. We first conducted a primary screen of 50 000 compounds to identify those that could suppress the

expression of a well-characterized EWS-FLI1 downstream target luciferase reporter construct. In the primary screen, we evaluated the library of compounds by using an EWS-FLI1 downstream target NR0B1 promoter luciferase construct in parallel with a constitutively active CMV promoter construct to control for nonspecific transcription inhibitors and a cell viability assay to control for nonspecific cytotoxins (Figure 1, A). This screen yielded compounds that inhibited expression of the target reporter construct but had no effect on the CMV reporter construct or on cell viability.

We then conducted a secondary screen of the 200 compounds to identify those that could directly suppress expression of multiple downstream targets of EWS-FLI1. We first generated a novel list of EWS-FLI1 downstream targets from four datasets comprising two clinical patient sample datasets and two experimental datasets. Genes that were highly expressed in ESFT patient tissue samples compared with normal tissue and other tumor types were selected. We subsequently included only those genes whose expression increased with EWS-FLI1 expression in the presumed cell of origin, mesenchymal progenitor cells (7,34–37). Finally, we included only the genes whose expression decreased with siRNA knockdown of EWS-FLI1 from a dataset in the literature (38). We selected the remaining genes that were in all four sets to give a preliminary list of 28 genes (Figure 1, B).

To generate the final list of genes used in the multiplex PCR assay, we selected nine of the targets from the preliminary list (see "Materials and Methods" for details); included two additional well-characterized targets, ID2 and CAV1, from the literature (39,40); a primer pair for EWS-FLI1 itself; and four different housekeeping genes to generate the final list of genes to use in the secondary screen (Supplementary Figure 2, available online).

Once the assays were designed and validated, we evaluated and prioritized 50 000 compounds based on the inhibition of the EWS-FLI1–specific promoter while maintaining expression of the CMV promoter yielding the top 200 compounds (see "Materials and Methods"). We eliminated all compounds that lost activity or selectivity with a 10-fold dilution and screened the remaining top 43 compounds by using the multiplex PCR EWS-FLI1 gene signature assay (summarized in Figure 1, C). We sorted these compounds mathematically using log-transformed data and plotted the data in a heat map format for visualization purposes only (Supplementary Figure 1, available online). The compound that showed the best suppression of the EWS-FLI1 gene signature, mithramycin, was selected for further study.

Effect of Mithramycin Treatment on the NR0B1- and CMV-Driven Luciferase Reporters

To examine the dose-dependent effect of mithramycin on expression of downstream targets at the promoter level, we treated TC32 cells containing the NR0B1- and CMV-driven luciferase reporter constructs for 6 hours over a range of concentrations from 200 to 5 nM and measured the effect on bioluminescence. Mithramycin decreased NR0B1 promoter activity in a dose-dependent fashion at concentrations between 5 and 200 nM at 6 hours without affecting the activity of the constitutively active CMV promoter. For example, treatment of TC32 cells with 50 nM mithramycin for 6 hours reduced luciferase expression to only 61% of control (95% CI = 57% to 65%) ($P < .001$) (Figure 2, A). At 6 hours, these effects could not be accounted for by a general reduction in transcription because there was only minimal change in CMV-driven luciferase activity or by cell death because no change in cell number was observed at this time point (data not shown). Similar results were obtained with replicate experiments at 6, 12, 24, and 48 hours of incubation (data not shown). However, the suppression of luciferase expression at the longer incubation times was confounded by an increase in cell death and therefore only the 6-hour time point is shown.

Effect of Mithramycin on EWS-FLI1 Gene Signatures

We confirmed the effect of mithramycin treatment on the novel EWS-FLI1 gene signature by incubating TC32 cells with 100 nM mithramycin for 6 hours and measuring the effect on the expression of EWS-FLI1 target genes using RT multiplex PCR (Figure 2, B). Mithramycin decreased the expression of 10 of the 11 EWS-FLI1 downstream target genes (all but *CCK*) but did not suppress expression of *GAPDH*. We confirmed the result of the multiplex PCR by performing quantitative RT-PCR for five genes: *CCK*, which did not suppress in the multiplex PCR; *NR0B1* and *ID2* (for which antibodies are available); and *RCOR1* and *LDB2* because their expression was decreased the most by mithramycin compared with control in the multiplex PCR assay. The data confirmed the results of the multiplex PCR: Mithramycin treatment did not change *CCK* expression but suppressed it for the other four targets relative to control ($P = .008$) (gene expression ratio for mithramycin-treated to control, *ID2*: 0.7, 95% CI = 0.56 to 0.90 [$P = .09$]; *LDB2*: 0.7, 95% CI = 0.49 to 0.84 [$P = .04$]; *NR0B1*: 0.4, 95% CI = 0.36 to 0.49 [$P = .01$]; *RCOR1*: 0.2, 95% CI = 0.08 to 0.31 [$P = .01$]) (Figure 2, C).

Next, to demonstrate suppression of an independent EWS-FLI1 gene signature, we evaluated a list of EWS-FLI1–induced targets from the literature (45). We performed microarray gene expression analysis on TC32 and TC71 cells treated with mithramycin or control and used GSEA (44) to investigate the enrichment of EWS-FLI1 target genes in mithramycin-treated cells. EWS-FLI1–induced target genes were statistically significantly enriched in the list of genes whose expression decreased with mithramycin treatment ($P < .001$) with a core set of 30 genes found in the leading edge subset that accounts for the enrichment signal (Figure 2, D). Finally, we used the geneSetTest function from the limma package as an alternative statistical method to confirm that mithramycin treatment suppressed expression of the list of EWS-FLI1 targets ($P < .001$) (43).

Effect of Mithramycin on Protein Expression of NR0B1 and ID2

Next, we evaluated the effect of mithramycin treatment on the protein expression of NR0B1 and ID2, which are generally accepted as EWS-FLI1 downstream targets (38,39,46) and for which reliable antibodies exist. In TC32 cells treated with 100 nM mithramycin, expression of both targets decreased between 6 and 12 hours of treatment (Figure 3, A). This time frame is consistent with the time frame of mRNA suppression detected by quantitative PCR (Figure 2, C) and occurs at the same time or just before the induction of apoptosis as determined by the cleavage of PARP.

In addition, we observed a clear dose-dependent inhibition of ID2 protein expression in both the TC32 and TC71 cell lines at 24 hours of treatment with 100 nM and 10 nM mithramycin (Figure 3, B). There was no change in expression of EWS-FLI1 in TC32 or TC71 cells treated with mithramycin at any concentration for any time.

Effects of Mithramycin on DNA Damage

Mithramycin is known to bind the minor groove of DNA (47). We therefore examined the effects of mithramycin treatment on the integrity of the DNA by treating TC32 cells with mithramycin and measuring the effect on p53 activation and on γH2AX formation. The phosphorylation of histone H2AX at serine 139 (ie, the generation of γH2AX) is known to occur at sites of DNA double-strand breaks and therefore marks DNA damage (48). We found that there is a secondary DNA damaging effect of mithramycin treatment that occurs after inhibiting the downstream target expression as measured by immunoblot analysis showing the activation and subsequent degradation of p53 and the phosphorylation of H2AX. At 12–18 hours of exposure, mithramycin caused the induction of phosphorylation at serine 15 and subsequent degradation of p53, which was complete by 48 hours (Figure 4, A). To confirm that the generation of γH2AX observed was not simply the result of an apoptotic effect, we performed confocal microscopy following mithramycin treatment. The γH2AX foci appeared in a diffuse nuclear pattern consistent with the accumulation of DNA double-strand breaks (48) in the mithramycin-treated cells but not the control cells at 24 hours following treatment (Figure 4, B). Finally, it is notable that p21 induction occurred before the phosphorylation of serine 15 of p53 and that no further increase in p21 expression occurred after activation of p53.

Effects of Mithramycin on Viability of a Panel of Cell Lines

To evaluate the effect of EWS-FLI1 suppression on cell viability, we treated a panel of cell lines for 48 hours with concentrations of mithramycin that ranged from 500 to 0.5 nM and measured the

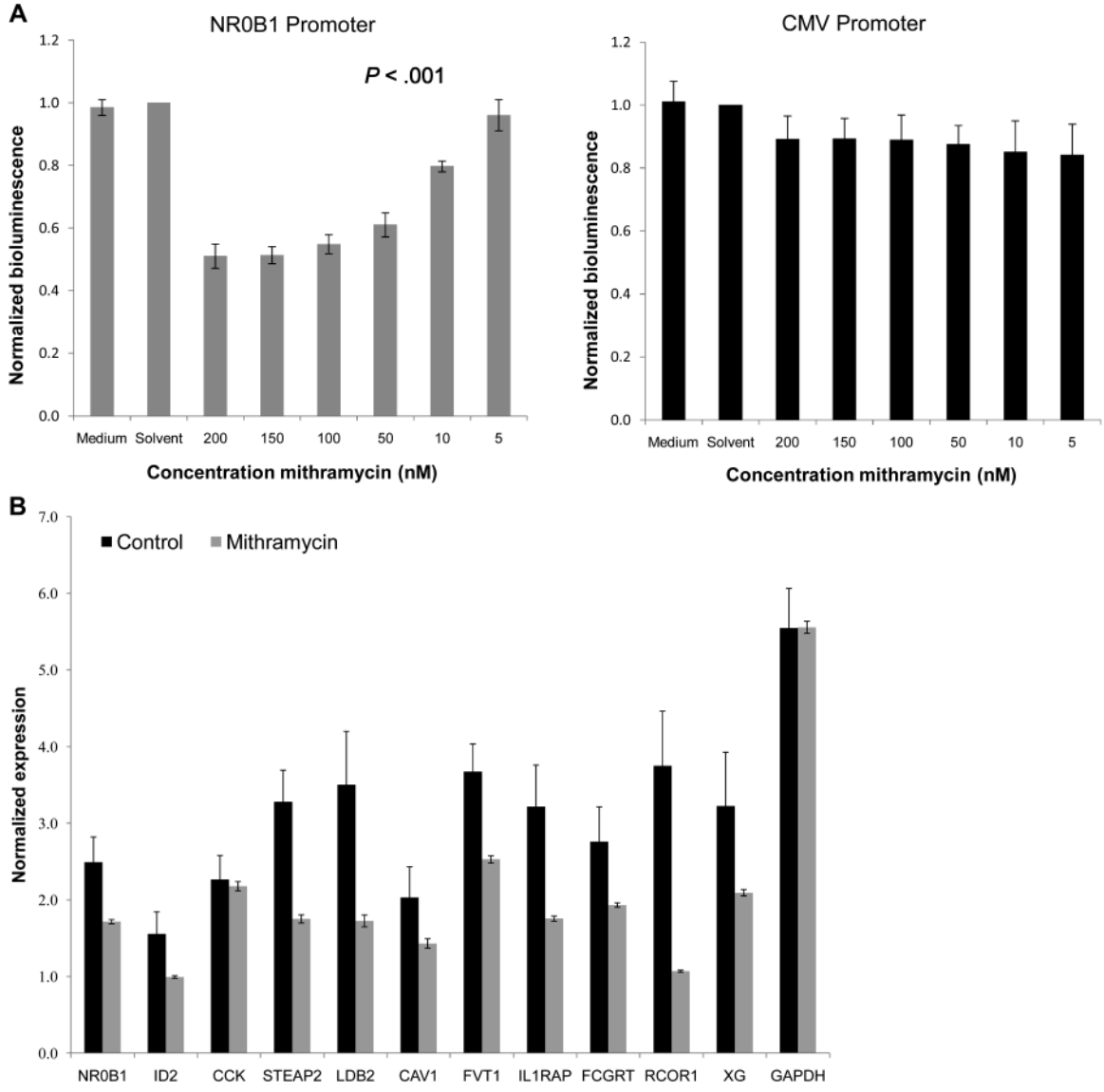

(continued)

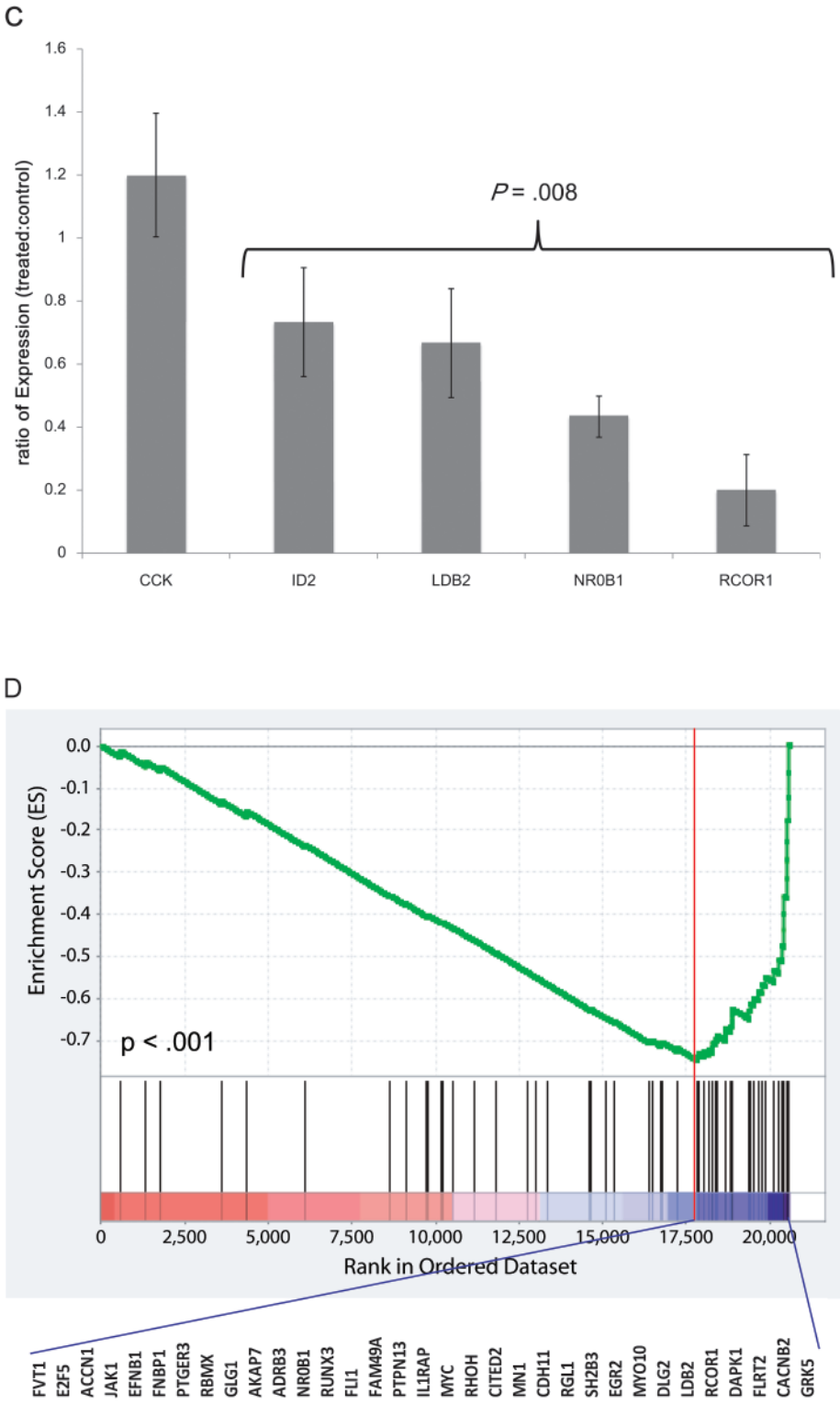

Figure 2. Effect of mithramycin on EWS-FLI1 downstream target expression. **A**) Luciferase reporter assay. TC32 cells bearing the NR0B1-driven luciferase reporter or the CMV (cytomegalovirus)-driven control promoter were incubated with mithramycin at concentrations ranging from 5 to 200 nM for 6 hours, and the bioluminescence was read after the addition of luciferin reagent. Data are normalized to the solvent control and represent the average of six replicates from a single experiment; **error bars** represent 95% confidence intervals. The Student *t* test was used to compare the statistical significance of the difference in mean expression between the CMV-driven luciferase and the NR0B1-driven luciferase in cells treated with 50 nM mithramycin (n = 6) ($P < .001$). **B**) EWS-FLI1 downstream target expression. TC32 cells bearing the NR0B1-driven luciferase reporter were treated with 100 nM mithramycin or solvent (control) for 6 hours, and expression of the downstream targets was assessed with the multiplex polymerase chain reaction (PCR) assay and normalized to an internal PCR control (Kan^r RNA). The data represent the average of three replicates from one experiment; **error bars** represent 95% confidence intervals. The housekeeping gene *GAPDH* is shown as an internal control. **C**) Quantitative PCR verification. RNA was collected from TC32 cells treated with 100 nM mithramycin for 6 hours at 37°C and analyzed by reverse transcription–quantitative PCR. Expression of each gene was evaluated as a function of a change in the expression of the *GAPDH* reference gene and plotted as the ratio of expression of the treated to control target gene. The data represent the average of eight replicates from three independent experiments. **Error bars** indicate the 95% confidence intervals. The *P* value represents the statistical significance of the difference between the treated and solvent control groups and was determined by the Student *t* test (two-sided). *CCK* was not included in the *t* test because there was no difference in *CCK* expression between the mithramycin-treated and solvent control samples. **D**) Enrichment plot of EWS-FLI1 target genes. TC32 cells were treated with 100 nM mithramycin for 6 hours. RNA was collected and gene expression was profiled using Affymetrix microarrays. Expression of EWS-FLI1–induced target genes was statistically significantly suppressed by mithramycin treatment compared with control ($P < .001$). Gene set enrichment analysis (44) was completed with weighted enrichment statistics and genes ranked using the $\log_2$ ratio of gene expression in mithramycin-treated and control cells as described in the "Material and Methods" section. The **black vertical lines** mark the hits of EWS-FLI1 target genes. The **red vertical line** specifies the maximum enrichment score, which reflects the degree to which a gene set is overrepresented at the bottom of a ranked list of genes. The genes listed under the plot are the leading-edge subset, which is a subset of EWS-FLI1–induced target genes that contribute most to the maximum enrichment score.

IC_{50} values. Mithramycin was a potent cytotoxic agent in a panel of ESFT cell lines, with IC_{50} values that ranged from 10 nM (95% CI = 8 to 13 nM) to 15 nM (95% CI = 13 to 19 nM) (Table 1). We also evaluated other solid tumor cell lines, including osteosarcoma, breast carcinoma, and ovarian carcinoma and found somewhat higher IC_{50} values. It is notable that all ESFT cell lines tested were extremely sensitive to the drug, and they were slightly more sensitive to mithramycin treatment than the other cell lines tested.

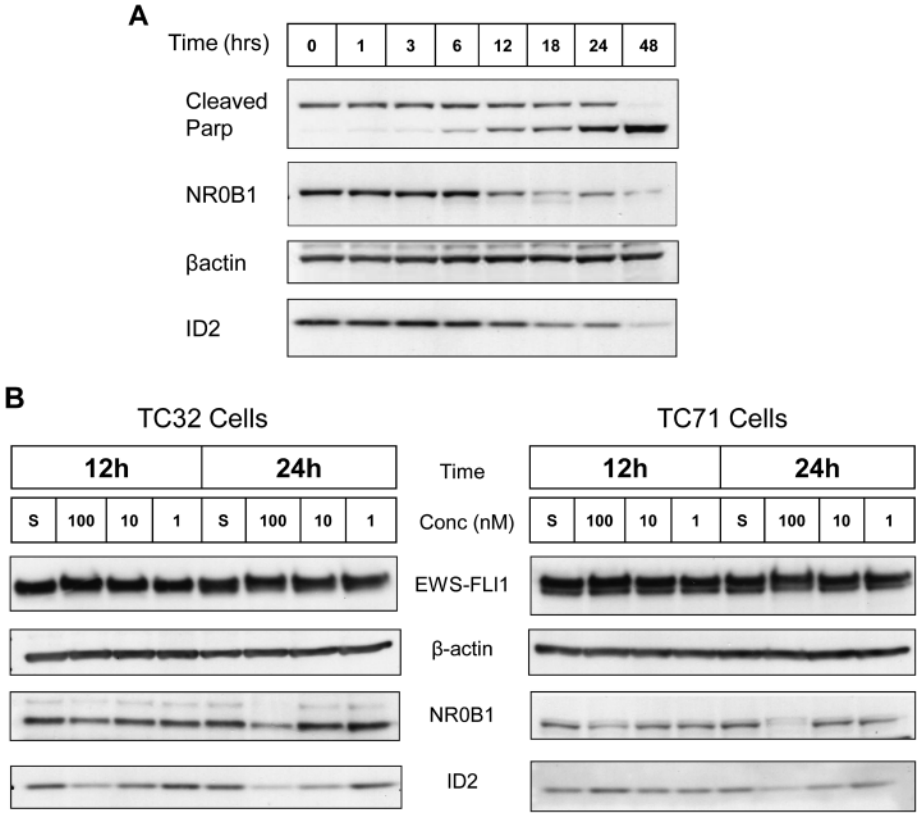

Figure 3. Immunoblot analysis of the EWS-FLI1 downstream targets NR0B1 and ID2. **A**) Time course of NR0B1 and ID2 protein expression and PARP cleavage. TC32 cells were incubated with 100 nM mithramycin. Protein lysates were made at various times of incubation and subjected to immunoblot analysis. PARP cleavage was used to indicate induction of apoptosis, and β-actin was used as a control for equal protein loading. Two repeat time course experiments verified these results. **B**) Dose-dependent effect of mithramycin treatment. TC32 (left) and TC71 (right) ESFT cells were treated with 100, 10, or 1 nM mithramycin for 12 or 24 hours. Protein lysates were collected and subjected to immunoblot analysis. Two repeat experiments yielded similar results in both TC71 and TC32 cells. S = solvent control; conc = concentration.

Effect of Mithramycin on Growth of ESFT and Osteosarcoma Xenografts

Next, we examined the effect of mithramycin on tumor growth in vivo using two different Ewing sarcoma xenografts and one osteosarcoma xenograft. In the first experiment, we defined the effective dose that did not result in substantial toxicity. Mice with TC71 xenografts were treated with mithramycin at four different doses every Monday, Wednesday, and Friday for 11 days; control mice received no treatment (n = 14–16 mice per group). The mice that were treated with the two highest doses of mithramycin—0.5 and 1.0 mg/kg body weight—had statistically significantly reduced growth of the TC71 xenografts compared with control ($P < .001$ for both). On day 10 of treatment, mean tumor volume was reduced by 47% in the 0.5 mg/kg dose group (control vs 0.5 mg/kg mithramycin: 2696 vs 1259 mm^3, difference = 1437 mm^3, 95% CI = 787 to 2087 mm^3) and by 75% in the 1.0 mg/kg dose group (control vs 1.0 mg/kg mithramycin: 2860 vs 686 mm^3, difference = 2174 mm^3, 95% CI = 1589 to 2770 mm^3) relative to the control tumor volume (Figure 5, A).

We also observed a statistically significant decrease in growth of the TC32 and TC71 xenografts over time in mice treated thrice weekly with mithramycin at 1.0 mg/kg body weight (n = 15 mice per group) (Figure 5, B). The TC32 xenografts showed profound tumor growth inhibition with a decrease in the mean tumor volume of the entire cohort after a single dose of mithramycin to almost no appreciable tumor in any of the mice that persisted with continued treatment. For example, on day 15 of treatment, whereas the mean tumor volume for the mithramycin-treated mice was only slightly less than mean volume at the start of treatment (69 vs 76 mm^3, difference = 7 mm^3, 95% CI = −13 to 27 mm^3, $P = .57$), it was approximately 3% of the tumor volume observed in the control mice (mithramycin vs control: 69 vs 2388 mm^3, difference = 2319 mm^3, 95% CI = 1766 to 2872 mm^3, $P < .001$). Only three of the 12 evaluable mithramycin-treated mice bearing TC32 xenografts had any appreciable tumor at day 19 of treatment, when all of the control mice had to be killed due to tumor progression to 2 cm (Figure 5, B). The TC71 xenografts in mice treated with mithramycin also showed a statistically significant suppression of tumor growth compared with control (mean tumor volume on day 15 of treatment for mithramycin vs control: 762 vs 3502 mm^3, difference = 2740 mm^3, 95% CI = 2329 to 3157 mm^3, $P < .001$), a volume roughly 22% of control, which translated into a near doubling in median survival from 15 to 26 days for mice bearing the TC71 xenograft (Figure 5, B and C).

As a control for nonspecific effects of mithramycin, we implanted a cohort of mice with the osteosarcoma MNNG-HOS cells, which lack the EWS-FLI1 translocation, and treated them by intraperitoneal injection with mithramycin at 1 mg/kg body weight per day, three times per week. Despite the relatively similar in vitro IC_{50} values for mithramycin in MNNG-HOS, TC32, and TC71 cells, mithramycin had less of an impact on the growth of the MNNG-HOS xenografts than it had on the EWS-FLI1–expressing TC32 and TC71 xenografts and no impact on the survival of the mice at the time when the surviving mice had to be euthanized (Figure 5, D).

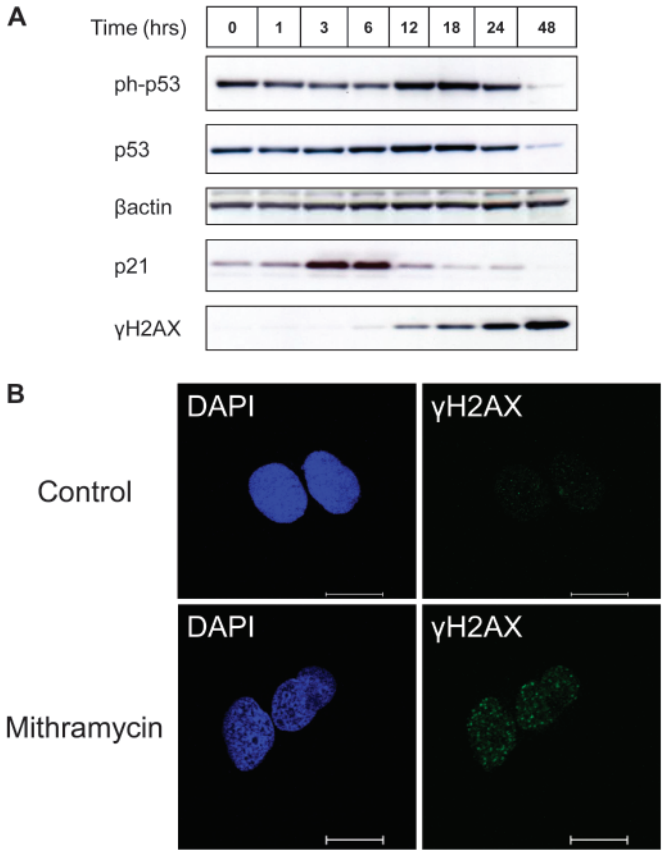

Figure 4. Effect of mithramycin on DNA damage response. **A**) Immunoblot analysis. TC32 cells were treated with 100 nM mithramycin. Cells were collected at the indicated times during incubation and used to make protein lysates, which were subjected to immunoblot analysis to assess the induction of the DNA damage response as reflected by the phosphorylation of H2AX (detected with a phosphorylation-specific antibody) and phosphorylation of serine 15 of p53 (ph -p53) and the subsequent degradation of p53. Similar results were obtained in repeat experiments. **B**) Confocal microscopy. TC32 cells were treated with 100 nM mithramycin or phosphate-buffered saline (control) for 24 hours and immunostained with an antibody that recognizes phosphorylated H2AX (γH2AX; **green**), counterstained with DAPI (**blue**) to image nuclei, and analyzed by confocal microscopy. Scale bars = 20 μm.

To confirm that the effects mithramycin on tumor growth were related to suppression of EWS-FLI1 activity, we used immunohistochemistry to examine the expression of NR0B1 in the TC71 xenograft. Hematoxylin- and eosin-stained sections of tumors resected on day 4 of treatment from both treated and control mice showed viable small round cells characteristic of ESFT (Figure 5, E). However, the tumors from control mice displayed nuclear and cytoplasmic staining with an antibody against NR0B1, whereas the tumors from mithramycin-treated mice showed almost no such staining (Figure 5, E). Similar to the results obtained in vitro, immunoblot analysis of tumor lysates revealed induction of apoptosis, as measured by the cleavage of PARP, and phosphorylation of H2AX by day 11 in the treated mice but not the control mice (Figure 5, F).

The mice tolerated mithramycin very well on the dose and schedule used in this study; we observed only minimal myelosuppression, liver enzyme elevations, and minor electrolyte abnormalities, which were not life threatening.

Table 1. IC_{50} values for mithramycin in human cancer cell lines*

Cell line	Cell type	Mean IC_{50}, nM (95% CI)
TC71	ESFT	10 (8 to 13)
A673	ESFT	10 (7 to 12)
TC167	ESFT	11 (11 to 11)
TC32	ESFT	15 (13 to 19)
EW8	ESFT	15 (14 to 19)
CHLA9	ESFT	15 (12 to 15)
MNNG-HOS	Osteosarcoma	21 (11 to 40)
U2OS	Osteosarcoma	35 (12 to 95)
MD-MBA-231	Breast cancer	20 (12 to 35)
MCF7	Breast cancer	70 (42 to 100)
SKOV3	Ovarian carcinoma	>500 (UTD)

* IC_{50} experiments were performed in 96-well plates using an MTS assay. Each cell line was assayed in 2–5 independent experiments. CI = confidence interval; ESFT = Ewing sarcoma family of tumors; IC_{50} = concentration that caused a 50% loss of cell viability compared with untreated control cells; UTD = unable to determine (because the cells did not achieve <1% viability even at concentrations >500 nM).

Discussion

In this study, we have used a novel screening method to identify mithramycin as an inhibitor of the EWS-FLI1 transcription factor. We showed that this drug blocks expression of EWS-FLI1 downstream targets in vitro at both the RNA and protein level and suppresses protein expression of a well-characterized downstream target, NR0B1, in vivo. Mithramycin inhibited ESFT cell growth in vitro with IC_{50} values ranging from 10 to 15 nM and suppressed the growth of ESFT xenografts in vivo to 3% of control in the more sensitive TC32 xenograft model of ESFT.

Ewing sarcoma is a malignant bone tumor of childhood with an extremely poor prognosis, particularly for high-risk patients. To improve patient outcomes, recent efforts have been aimed at developing therapies targeting the EWS-FLI1 oncogenic transcription factor that characterizes this disease (19,20). This goal stems from the widely validated dependence of this tumor on the continued expression of EWS-FLI1 to maintain the malignant phenotype. Most notably, a gene signature approach has been used to identify cytosine arabinoside as an inhibitor of EWS-FLI1 (19). Another investigation characterized an interaction between EWS-FLI1 and RNA helicase A and used high-throughput screening to identify a small molecule (YK-4-279) that blocks this protein–protein interaction to disrupt EWS-FLI1 activity (20). To date, neither cytosine arabinoside nor YK-4-279 has shown activity in the clinic.

The idea of targeting oncogenic transcription factors with small-molecule inhibitors is attractive from both a theoretical and a practical perspective. Aside from the likely dependence of a variety of carcinomas, sarcomas, and leukemia on specific fusion transcription factors, the success of all-*trans* retinoic acid and arsenic for the treatment of high-risk acute promyelocytic leukemia and ET-743 for myxoid liposarcoma offers further evidence for optimism regarding transcription factor–targeted small molecules (49–55). In both cases, the dramatic responses that have been observed in the clinic are likely due to inhibition of the oncogenic fusion transcription factor responsible for oncogenesis and progression for the individual tumor (56–58). However, it was only after these drugs were found to have activity in the clinic that the

mechanism was determined to be interference with the activity of the oncogenic fusion transcription factor.

We have developed a novel method to screen for transcription factor inhibitors with the goal of inhibiting EWS-FLI1 in ESFT. The method combines an EWS-FLI1 downstream target promoter reporter cell-based screen with a gene signature multiplex PCR approach. The assays proved to be robust enough to evaluate a large library of more than 50 000 compounds and yet specific enough to allow us to successfully identify and characterize the compound mithramycin as an inhibitor of EWS-FLI1. The ultimate validation of both the method and the drug is the observed response of the TC32 xenograft to drug treatment.

Like most natural products, mithramycin appears to work by multiple mechanisms in ESFT cells. First and foremost, mithramycin inhibits the transcriptional activity of EWS-FLI1 as measured by suppression of two different gene signatures and specific well-established downstream targets both in vitro and in vivo. The mechanism of this transcriptional interference likely occurs at the promoter level. Mithramycin is known to bind DNA and suppress the activity of specific transcription factors, most notably SP1. It is known that SP1 cooperates with members of the E26 transformation-specific (ETS) family of transcription factors, including FLI1, to both activate and suppress expression of downstream targets (59–63). In addition, SP1 and EWS-FLI1 have been shown to cooperate to activate the *VEGF* and *CCND1* promoters (64). This cooperative activity is only partially blocked by mutating the SP1-binding sites in the *CCND1* promoter, which suggests that the activity of both EWS-FLI1 and SP1 is important for the transcription of *CCND1* (64). Currently, it is unclear whether the EWS-FLI1 suppression reported here results from the direct blockage of EWS-FLI1 binding, SP1 binding, or both, and ongoing experiments are aimed at answering this question.

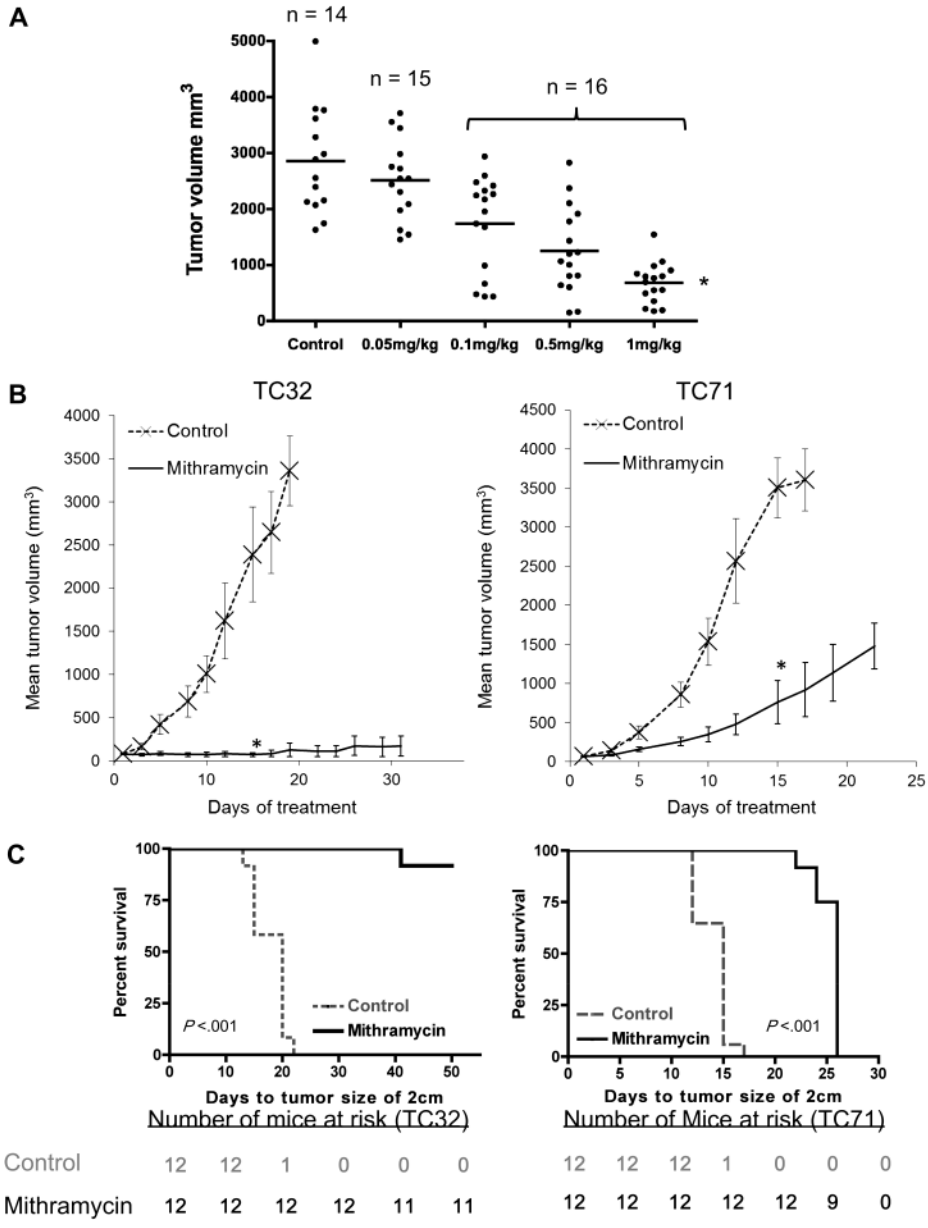

(continued)

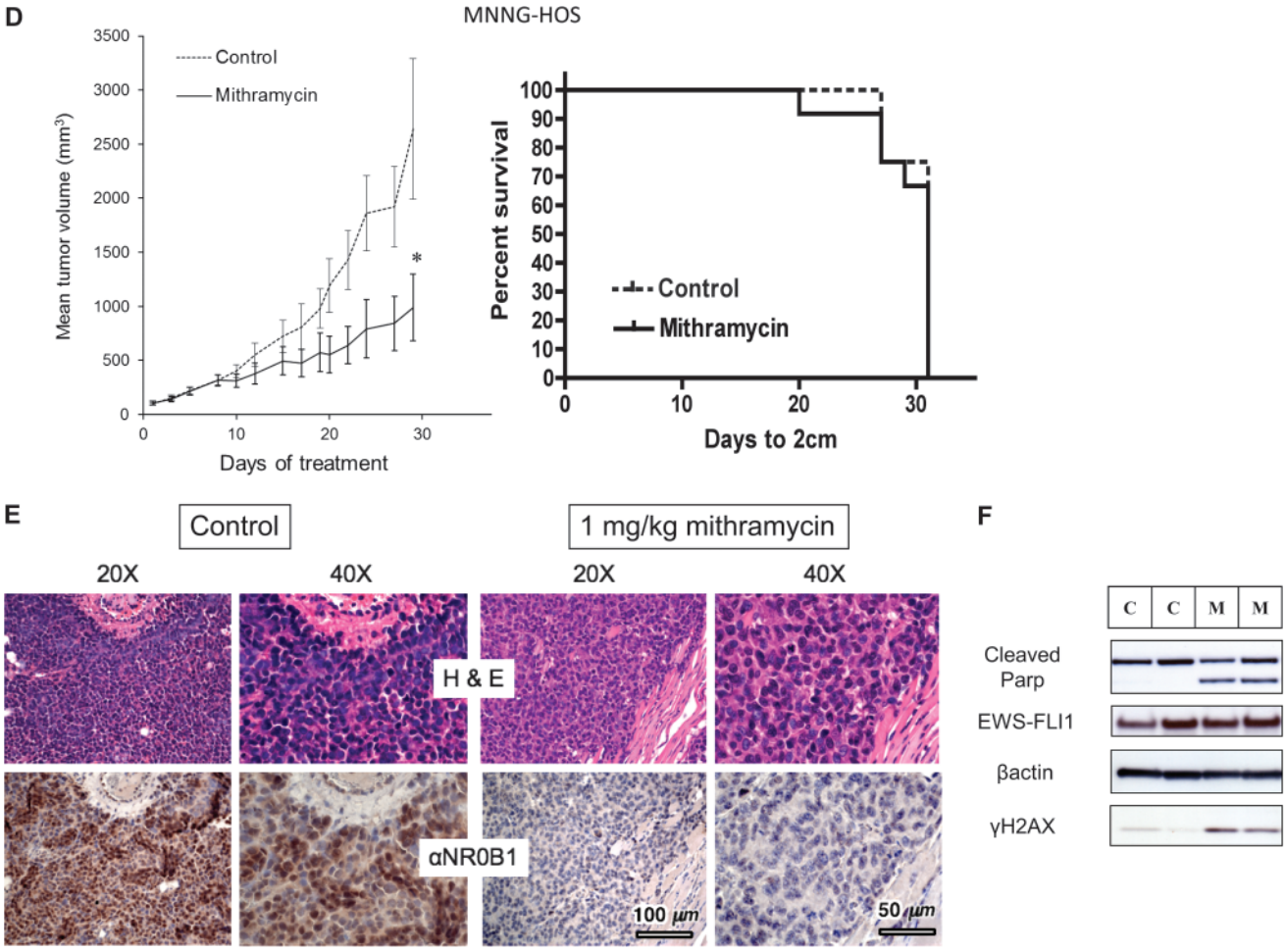

Figure 5. Effect of mithramycin on mice harboring TC32 and TC71 ESFT and MNNG-HOS osteosarcoma xenografts. **A**) Dose–response effect in mice bearing TC71 xenografts on day 11. Mice were treated with the mithramycin at the dose specified on the *x*-axis on a Monday-Wednesday-Friday (M-W-F) schedule for 11 days and killed when the tumor reached 2 cm. Control mice were untreated (n = 20 mice per group). Each **dot** represents the tumor of an individual mouse of the possible 16 in each cohort treated with mithramycin (four mice from each group were killed according to a predefined schedule to collect tissue for biochemical analysis). The **horizontal lines** represent mean values. The number of mice remaining in each cohort is specified above each column. There were fewer mice in control and 0.5 mg/kg groups because the tumors in some of those mice reached the allowable maximum size, necessitating killing. The **asterisk** indicates statistically significant difference in mean tumor volume for the 1 mg/kg body weight per dose cohort vs the control group ($P < .001$, two-sided Student *t* test). **B**) Growth of ESFT xenografts. Mice were injected into the left gastrocnemius muscle with TC32 or TC71 ESFT cells and tumors were allowed to establish. Mice were subsequently randomly assigned to the treatment (n = 15) or control (n = 15) group; treated mice received mithramycin by intraperitoneal injection at a dose of 1 mg/kg body weight dose on a M-W-F schedule, and control mice were untreated. The **curves** represent the mean tumor volume for mice bearing the TC32 (left) or TC71 (right) xenografts and **error bars** represent 95% confidence intervals. The **asterisks** indicate a statistically significant difference in tumor volumes on day 15 between the treatment and control groups ($P < .001$ for both; two-sided Student *t* test). **C**) Kaplan–Meier survival curves of mice bearing ESFT xenografts. The survival of the mice treated as described above is shown for the mithramycin-treated mice bearing either the TC32 (left) or TC71 (right) xenografts compared with the control cohort. **D**) Growth of MNNG-HOS osteosarcoma xenografts and survival of mice bearing these tumors. Mice were implanted with MNNG-HOS xenografts and, once tumors were established, randomly assigned to receive mithramycin by intraperitoneal injection at a dose of 1 mg/kg body weight dose on a M-W-F schedule or no treatment (control) (n = 15 mice per group). Mean tumor volumes (left) and the survival curves (right) are shown; **error bars** represent 95% confidence intervals. The **asterisk** indicates a statistically significant difference in tumor volumes on day 30 between the treatment and control groups ($P < .001$; two-sided Student *t* test). **E**) Immunohistochemical analysis of TC71 xenograft tumors. Mice bearing TC71 xenograft tumors were treated with mithramycin at 1 mg/kg per dose on day 1 or not treated (control) and tumor tissue collected on day 4. Tumor sections were stained with hematoxylin–eosin (upper panels) and immunostained for NR0B1 (**brown**, lower panels). The 20× and 40× fields shown are representative of the entire section. Similar results were obtained by staining another section. **F**) Immunoblot analysis of TC71 xenograft tumor lysates. Tumors were collected from control (C) and mithramycin-treated mice (M), 11 days after intraperitoneal treatment with mithramycin on an M-W-F schedule was initiated. The lysates shown were collected from two different control mice and two different mice in the 1 mg/kg per dose cohort.

We also demonstrated that mithramycin induces DNA damage in ESFT cells as measured by the phosphorylation and degradation of p53 and the generation of γH2AX foci. To our knowledge, this is the first report of mithramycin inducing DNA damage in a cell. In ESFT cells, the relative contribution of this DNA damage to the apoptotic process is not clear, given that it has been shown by chromatin immunoprecipitation that mithramycin blocks the activation of the downstream effectors of p53, namely PUMA, Bak, and p21, via an SP1-dependent mechanism (65). The effects of mithramycin on p21 expression are particularly notable because

EWS-FLI1 has also been shown to suppress p21 expression by binding to the promoter (65,66). We showed that treatment of ESFT cells with mithramycin-induced expression of p21 within 1–3 hours, consistent with a release of EWS-FLI1–mediated repression of p21. However, no increase in expression of p21 occurred with p53 activation as would be expected with DNA damage, suggesting that these cells have either a mutated p53 or a downstream mithramycin-mediated block in expression of p21 in the setting of p53 activation.

We found that mithramycin is highly cytotoxic to ESFT cells in vitro, with IC_{50} values of 10–15 nM in a panel of ESFT cell lines. We found that mithramycin was slightly more cytotoxic to the ESFT cell lines than the other cell lines tested particularly when compared with the carcinoma cell lines. It is notable that the TC32, TC71, and MNNG-HOS osteosarcoma cells had relatively similar IC_{50} values in vitro with a one- to twofold increase in cytotoxicity observed in the ESFT cell lines compared with the osteosarcoma MNNG-HOS cell line.

On the other hand, the selective cytotoxicity of mithramycin for ESFT cell lines was more pronounced in vivo. For example, the MNNG-HOS osteosarcoma xenograft displayed limited tumor growth suppression and no improvement in survival for the mice treated with mithramycin. By contrast, both ESFT xenografts showed a pronounced and sustained suppression of tumor growth with mithramycin treatment that translated into prolonged survival. We believe the in vivo selectivity of mithramycin for ESFT comes not from the drug but from the dependence of this tumor on the target, EWS-FLI1. The reasons for the observed differences in tumor growth between the two ESFT xenografts treated with mithramycin are of interest and may reflect the marked tumor heterogeneity that exists both between genetically similar tumors as well as within a single tumor.

Mithramycin was originally evaluated as an antitumor agent in the clinic during the 1960s. Although mithramycin showed some promise in patients with testicular cancer, it was not pursued likely due to the development of other successful treatment regimens as well as limitations in supportive care during that era that hindered management of the side effects of mithramycin (67). Mithramycin was also tested for the treatment of Ewing sarcoma (68,69). At least two of five Ewing sarcoma patients treated with mithramycin achieved widespread clinical responses, and one patient with metastatic disease achieved a durable complete response lasting at least 7 years following a course of mithramycin as a single agent (69). Despite these impressive early clinical results, it is unclear why the use of mithramycin for Ewing sarcoma was abandoned. Nevertheless, the strong dependence of ESFT cells on EWS-FLI1 coupled with the evidence in this report that mithramycin inhibits expression of EWS-FLI1 downstream targets, when considered in light of these clinical case reports of patients responding to treatment, strongly suggest a potential role for mithramycin in the treatment of Ewing sarcoma. We are therefore currently obtaining clinical grade mithramycin to open a clinical trial and reinvestigate this drug for the treatment of ESFT.

The major limitation of this study is that the screen and subsequent experiments were all conducted in cell lines and xenografts of those cell lines. Furthermore, we did not verify the authenticity of the non-ESFT cell lines used in this study. In addition, the investigators were not blinded to the treatment groups in the mouse experiments, and only one assay (PARP cleavage) was performed to detect apoptosis. Finally, the multiplex PCR was repeated only one time and the findings were instead verified by alternative methods; the quantitative PCR and microarray experiments both of which confirmed the results in three independent experiments each.

References

1. Helman LJ, Meltzer P. Mechanisms of sarcoma development. *Nat Rev Cancer.* 2003;3(9):685–694.
2. Martens JH, Stunnenberg HG. The molecular signature of oncofusion proteins in acute myeloid leukemia. *FEBS Lett.* 2010;584(12):2662–2669.
3. Prensner JR, Chinnaiyan AM. Oncogenic gene fusions in epithelial carcinomas. *Curr Opin Genet Dev.* 2009;19(1):82–91.
4. Delattre O, Zucman J, Plougastel B, et al. Gene fusion with an ETS DNA-binding domain caused by chromosome translocation in human tumours. *Nature.* 1992;359(6391):162–165.
5. Delattre O, Zucman J, Melot T, et al. The Ewing family of tumors—a subgroup of small-round-cell tumors defined by specific chimeric transcripts. *N Engl J Med.* 1994;331(5):294–299.
6. Bailly RA, Bosselut R, Zucman J, et al. DNA-binding and transcriptional activation properties of the EWS-FLI-1 fusion protein resulting from the t(11;22) translocation in Ewing sarcoma. *Mol Cell Biol.* 1994;14(5):3230–3241.
7. Kauer M, Ban J, Kofler R, et al. A molecular function map of Ewing's sarcoma. *PLoS One.* 2009;4(4):e5415.
8. May WA, Gishizky ML, Lessnick SL, et al. Ewing sarcoma 11;22 translocation produces a chimeric transcription factor that requires the DNA-binding domain encoded by FLI1 for transformation. *Proc Natl Acad Sci U S A.* 1993;90(12):5752–5756.
9. Tanaka K, Iwakuma T, Harimaya K, Sato H, Iwamoto Y. EWS-Fli1 antisense oligodeoxynucleotide inhibits proliferation of human Ewing's sarcoma and primitive neuroectodermal tumor cells. *J Clin Invest.* 1997;99(2):239–247.
10. Maksimenko A, Malvy C. Oncogene-targeted antisense oligonucleotides for the treatment of Ewing sarcoma. *Expert Opin Ther Targets.* 2005;9(4):825–830.
11. Truong AH, Ben-David Y. The role of Fli-1 in normal cell function and malignant transformation. *Oncogene.* 2000;19(55):6482–6489.
12. May WA, Arvand A, Thompson AD, Braun BS, Wright M, Denny CT. EWS/FLI1-induced manic fringe renders NIH 3T3 cells tumorigenic. *Nat Genet.* 1997;17(4):495–497.
13. Eliazer S, Spencer J, Ye D, Olson E, Ilaria RL Jr. Alteration of mesodermal cell differentiation by EWS/FLI-1, the oncogene implicated in Ewing's sarcoma. *Mol Cell Biol.* 2003;23(2):482–492.
14. Richter GH, Plehm S, Fasan A, et al. EZH2 is a mediator of EWS/FLI1 driven tumor growth and metastasis blocking endothelial and neuroectodermal differentiation. *Proc Natl Acad Sci U S A.* 2009;106(13):5324–5329.
15. Toretsky JA, Kalebic T, Blakesley V, LeRoith D, Helman LJ. The insulin-like growth factor-I receptor is required for EWS/FLI-1 transformation of fibroblasts. *J Biol Chem.* 1997;272(49):30822–30827.
16. Kovar H, Aryee DN, Jug G, et al. EWS/FLI-1 antagonists induce growth inhibition of Ewing tumor cells in vitro. *Cell Growth Differ.* 1996;7(4):429–437.
17. Dohjima T, Lee NS, Li H, Ohno T, Rossi JJ. Small interfering RNAs expressed from a Pol III promoter suppress the EWS/Fli-1 transcript in an Ewing sarcoma cell line. *Mol Ther.* 2003;7(6):811–816.
18. Toretsky JA, Connell Y, Neckers L, Bhat NK. Inhibition of EWS-FLI-1 fusion protein with antisense oligodeoxynucleotides. *J Neurooncol.* 1997;31(1–2):9–16.
19. Stegmaier K, Wong JS, Ross KN, et al. Signature-based small molecule screening identifies cytosine arabinoside as an EWS/FLI modulator in Ewing sarcoma. *PLoS Med.* 2007;4(4):e122.
20. Erkizan HV, Kong Y, Merchant M, et al. A small molecule blocking oncogenic protein EWS-FLI1 interaction with RNA helicase A inhibits growth of Ewing's sarcoma. *Nat Med.* 2009;15(7):750–756.

21. Lombo F, Menendez N, Salas JA, Mendez C. The aureolic acid family of antitumor compounds: structure, mode of action, biosynthesis, and novel derivatives. *Appl Microbiol Biotechnol.* 2006;73(1):1–14.
22. Ward DC, Reich E, Goldberg IH. Base specificity in the interaction of polynucleotides with antibiotic drugs. *Science.* 1965;149(689):1259–1263.
23. Remsing LL, Bahadori HR, Carbone GM, McGuffie EM, Catapano CV, Rohr J. Inhibition of c-src transcription by mithramycin: structure-activity relationships of biosynthetically produced mithramycin analogues using the c-src promoter as target. *Biochemistry.* 2003;42(27):8313–8324.
24. Baker VV, Shingleton HM, Hatch KD, Miller DM. Selective inhibition of c-myc expression by the ribonucleic acid synthesis inhibitor mithramycin. *Am J Obstet Gynecol.* 1988;158(4):762–767.
25. Tagashira M, Kitagawa T, Nozato N, et al. Two novel C-glycosides of aureolic acid repress transcription of the MDR1 gene. *Chem Pharm Bull (Tokyo).* 2000;48(4):575–578.
26. Snyder RC, Ray R, Blume S, Miller DM. Mithramycin blocks transcriptional initiation of the c-myc P1 and P2 promoters. *Biochemistry.* 1991; 30(17):4290–4297.
27. Van Valen F. *Human Cell Culture.* London, UK: Kluwer; 1999.
28. Kim SY, Lee CH, Midura BV, et al. Inhibition of the CXCR4/CXCL12 chemokine pathway reduces the development of murine pulmonary metastases. *Clin Exp Metastasis.* 2008;25(3):201–211.
29. Palmieri D, Halverson DO, Ouatas T, et al. Medroxyprogesterone acetate elevation of Nm23-H1 metastasis suppressor expression in hormone receptor-negative breast cancer. *J Natl Cancer Inst.* 2005;97(9):632–642.
30. Thompson EW, Brunner N, Torri J, et al. The invasive and metastatic properties of hormone-independent but hormone-responsive variants of MCF-7 human breast cancer cells. *Clin Exp Metastasis.* 1993;11(1): 15–26.
31. Smith MA, Morton CL, Phelps D, Girtman K, Neale G, Houghton PJ. SK-NEP-1 and Rh1 are Ewing family tumor lines. *Pediatr Blood Cancer.* 2008;50(3):703–706.
32. Woldemichael GM, Vasselli JR, Gardella RS, McKee TC, Linehan WM, McMahon JB. Development of a cell-based reporter assay for screening of inhibitors of hypoxia-inducible factor 2-induced gene expression. *J Biomol Screen.* 2006;11(6):678–687.
33. Zhang JH, Chung TD, Oldenburg KR. A simple statistical parameter for use in evaluation and validation of high throughput screening assays. *J Biomol Screen.* 1999;4(2):67–73.
34. Riggi N, Suva ML, Suva D, et al. EWS-FLI-1 expression triggers a Ewing's sarcoma initiation program in primary human mesenchymal stem cells. *Cancer Res.* 2008;68(7):2176–2185.
35. Riggi N, Cironi L, Provero P, et al. Development of Ewing's sarcoma from primary bone marrow-derived mesenchymal progenitor cells. *Cancer Res.* 2005;65(24):11459–11468.
36. Castillero-Trejo Y, Eliazer S, Xiang L, Richardson JA, Ilaria RL Jr. Expression of the EWS/FLI-1 oncogene in murine primary bone-derived cells results in EWS/FLI-1-dependent, ewing sarcoma-like tumors. *Cancer Res.* 2005;65(19):8698–8705.
37. Tirode F, Laud-Duval K, Prieur A, Delorme B, Charbord P, Delattre O. Mesenchymal stem cell features of Ewing tumors. *Cancer Cell.* 2007;11(5): 421–429.
38. Kinsey M, Smith R, Lessnick SL. NR0B1 is required for the oncogenic phenotype mediated by EWS/FLI in Ewing's sarcoma. *Mol Cancer Res.* 2006;4(11):851–859.
39. Nishimori H, Sasaki Y, Yoshida K, et al. The Id2 gene is a novel target of transcriptional activation by EWS-ETS fusion proteins in Ewing family tumors. *Oncogene.* 2002;21(54):8302–8309.
40. Tirado OM, Mateo-Lozano S, Villar J, et al. Caveolin-1 (CAV1) is a target of EWS/FLI-1 and a key determinant of the oncogenic phenotype and tumorigenicity of Ewing's sarcoma cells. *Cancer Res.* 2006;66(20): 9937–9947.
41. Pfaffl MW. A new mathematical model for relative quantification in real-time RT-PCR. *Nucleic Acids Res.* 2001;29(9):e45.
42. Gautier L, Cope L, Bolstad BM, Irizarry RA. affy—analysis of Affymetrix GeneChip data at the probe level. *Bioinformatics.* 2004;20(3):307–315.
43. Smyth G. Limma: linear models for microarray data. In: Gentleman R, Carey V, Dudoit S, Irizarry R, Huber W, eds. *Bioinformatics and Computational Biology Solutions Using R and Bioconductor*. New York, NY: Springer; 2005: 397–420.
44. Subramanian A, Tamayo P, Mootha VK, et al. Gene set enrichment analysis: a knowledge-based approach for interpreting genome-wide expression profiles. *Proc Natl Acad Sci U S A.* 2005;102(43):15545–15550.
45. Hancock JD, Lessnick SL. A transcriptional profiling meta-analysis reveals a core EWS-FLI gene expression signature. *Cell Cycle.* 2008;7(2): 250–256.
46. Mendiola M, Carrillo J, Garcia E, et al. The orphan nuclear receptor DAX1 is up-regulated by the EWS/FLI1 oncoprotein and is highly expressed in Ewing tumors. *Int J Cancer.* 2006;118(6):1381–1389.
47. Banville DL, Keniry MA, Shafer RH. NMR investigation of mithramycin A binding to d(ATGCAT)2: a comparative study with chromomycin A3. *Biochemistry.* 1990;29(39):9294–9304.
48. Bonner WM, Redon CE, Dickey JS, et al. GammaH2AX and cancer. *Nat Rev Cancer.* 2008;8(12):957–967.
49. Hu J, Liu YF, Wu CF, et al. Long-term efficacy and safety of all-trans retinoic acid/arsenic trioxide-based therapy in newly diagnosed acute promyelocytic leukemia. *Proc Natl Acad Sci U S A.* 2009;106(9): 3342–3347.
50. Tallman MS. Treatment of relapsed or refractory acute promyelocytic leukemia. *Best Pract Res Clin Haematol.* 2007;20(1):57–65.
51. Casali PG, Sanfilippo R, D'Incalci M. Trabectedin therapy for sarcomas. *Curr Opin Oncol.* 2010;22(4):342–346.
52. Garcia-Carbonero R, Supko JG, Manola J, et al. Phase II and pharmacokinetic study of ecteinascidin 743 in patients with progressive sarcomas of soft tissues refractory to chemotherapy. *J Clin Oncol.* 2004;22(8):1480–1490.
53. Grosso F, Jones RL, Demetri GD, et al. Efficacy of trabectedin (ecteinascidin-743) in advanced pretreated myxoid liposarcomas: a retrospective study. *Lancet Oncol.* 2007;8(7):595–602.
54. Le Cesne A, Blay JY, Judson I, et al. Phase II study of ET-743 in advanced soft tissue sarcomas: a European Organisation for the Research and Treatment of Cancer (EORTC) soft tissue and bone sarcoma group trial. *J Clin Oncol.* 2005;23(3):576–584.
55. Delaloge S, Yovine A, Taamma A, et al. Ecteinascidin-743: a marine-derived compound in advanced, pretreated sarcoma patients–preliminary evidence of activity. *J Clin Oncol.* 2001;19(5):1248–1255.
56. Zhu J, Gianni M, Kopf E, et al. Retinoic acid induces proteasome-dependent degradation of retinoic acid receptor alpha (RARalpha) and oncogenic RARalpha fusion proteins. *Proc Natl Acad Sci U S A.* 1999;96(26): 14807–14812.
57. Zhu J, Koken MH, Quignon F, et al. Arsenic-induced PML targeting onto nuclear bodies: implications for the treatment of acute promyelocytic leukemia. *Proc Natl Acad Sci U S A.* 1997;94(8):3978–3983.
58. Forni C, Minuzzo M, Virdis E, et al. Trabectedin (ET-743) promotes differentiation in myxoid liposarcoma tumors. *Mol Cancer Ther.* 2009; 8(2):449–457.
59. Turner EC, Kinsella BT. Transcriptional regulation of the human prostacyclin receptor gene is dependent on Sp1, PU.1 and Oct-1 in megakaryocytes and endothelial cells. *J Mol Biol.* 2009;386(3):579–597.
60. Hempel N, Wang H, LeCluyse EL, McManus ME, Negishi M. The human sulfotransferase SULT1A1 gene is regulated in a synergistic manner by Sp1 and GA binding protein. *Mol Pharmacol.* 2004;66(6): 1690–1701.
61. Lu N, Heuchel R, Barczyk M, Zhang WM, Gullberg D. Tandem Sp1/Sp3 sites together with an Ets-1 site cooperate to mediate alpha11 integrin chain expression in mesenchymal cells. *Matrix Biol.* 2006;25(2): 118–129.
62. Jinnin M, Ihn H, Asano Y, Yamane K, Trojanowska M, Tamaki K. Tenascin-C upregulation by transforming growth factor-beta in human dermal fibroblasts involves Smad3, Sp1, and Ets1. *Oncogene.* 2004;23(9): 1656–1667.
63. Ahn J, Ko M, Lee K, Oh J, Jeon SH, Seong RH. Expression of SRG3, a core component of mouse SWI/SNF chromatin-remodeling complex, is regulated by cooperative interactions between Sp1/Sp3 and Ets transcription factors. *Biochem Biophys Res Commun.* 2005;338(3):1435–1446.
64. Fuchs B, Inwards CY, Janknecht R. Vascular endothelial growth factor expression is up-regulated by EWS-ETS oncoproteins and Sp1 and may

represent an independent predictor of survival in Ewing's sarcoma. *Clin Cancer Res.* 2004;10(4):1344–1353.
65. Koutsodontis G, Kardassis D. Inhibition of p53-mediated transcriptional responses by mithramycin A. *Oncogene.* 2004;23(57):9190–9200.
66. Nakatani F, Tanaka K, Sakimura R, et al. Identification of p21WAF1/CIP1 as a direct target of EWS-Fli1 oncogenic fusion protein. *J Biol Chem.* 2003;278(17):15105–15115.
67. Kennedy BJ, Torkelson JL. Long-term follow-up of stage III testicular carcinoma treated with mithramycin (plicamycin). *Med Pediatr Oncol.* 1995;24(5):327–328.
68. Kofman S, Medrek TJ, Alexander RW. Mithramycin in the treatment of embryonal cancer. *Cancer.* 1964;17(7):938–948.
69. Kofman S, Perlia CP, Economou SG. Mithramycin in the treatment of metastatic Ewing's sarcoma. *Cancer.* 1973;31(4):889–893.

Funding

This project has been funded in whole or in part with federal funds from the National Cancer Institute, National Institutes of Health, under contract N01-CO-12400. This research was supported in part by the Intramural Research Program of the NIH, National Cancer Institute, Center for Cancer Research. Grant support received from the Sarcoma Alliance for Research through Collaboration Career Development Award (to P.J.G.).

Notes

We would like to thank Susan Garfield for help with the confocal microscopy experiments, Xiaolin Wu for hybridizing and staining the microarrays, Carly Smith and Su Young Kim for help with the immunohistochemistry, Rick Dreyfuss for obtaining the immunohistochemistry images, Yves Pommier for helpful discussions, and Kathryn Sciabica for assistance developing the multiplex PCR assay. The content of this publication does not necessarily reflect the views or policies of the Department of Health and Human Services, nor does mention of trade names, commercial products, or organizations imply endorsement by the US Government. The funders had no role in the design of the study; the collection, analysis, and interpretation of the data; the decision to submit the article for publication; or the writing of the article.

Affiliations of authors: Molecular Oncology Section (PJG, LBG, CY, LJH), Tumor and Metastasis Biology Section (AM, CK), Oncogenomics Section (Q-RC, JK), Pediatric Oncology Branch, Center for Cancer Research, National Cancer Institute, National Institutes of Health, Bethesda, MD; Molecular Targets Laboratory, SAIC-Frederick Inc, National Cancer Institute, Frederick, MD (GMW); Department of Physiology, Johns Hopkins University School of Medicine, Baltimore, MD (DGC); Genetics Branch, Center for Cancer Research, National Cancer Institute, National Institutes of Health, Bethesda, MD (SD); Molecular Targets Laboratory, National Cancer Institute, Center for Cancer Research, Frederick, MD (JBM).